

# Multiple projection MCMC algorithms on submanifolds

Tony Lelièvre<sup>1</sup>, Gabriel Stoltz<sup>1</sup> and Wei Zhang<sup>2</sup>

<sup>1</sup> : Université Paris-Est, CERMICS (ENPC), Inria, F-77455 Marne-la-Vallée, France; {tony.lelievre,gabriel.stoltz}@enpc.fr

<sup>2</sup> : Zuse Institute Berlin, Takustrasse 7, 14195 Berlin, Germany; wei.zhang@fu-berlin.de

## Abstract

We propose new Markov Chain Monte Carlo algorithms to sample probability distributions on submanifolds, which generalize previous methods by allowing the use of set-valued maps in the proposal step of the MCMC algorithms. The motivation for this generalization is that the numerical solvers used to project proposed moves to the submanifold of interest may find several solutions. We show that the new algorithms indeed sample the target probability measure correctly, thanks to some carefully enforced reversibility property. We demonstrate the interest of the new MCMC algorithms on illustrative numerical examples.

**Keywords** Markov chain Monte Carlo, hybrid Monte Carlo, submanifold, constrained sampling.

## 1 Introduction

Sampling probability distributions on submanifolds is relevant in various applications. In molecular dynamics and computational statistics for instance, one is often interested in sampling probability distributions on the (zero) level set of some lower-dimensional function  $\xi : \mathbb{R}^d \rightarrow \mathbb{R}^k$ , where  $1 \leq k < d$ :

$$\Sigma = \{x \in \mathbb{R}^d \mid \xi(x) = 0 \in \mathbb{R}^k\} . \quad (1)$$

The function  $\xi$  corresponds in molecular dynamics to molecular constraints (fixed bond lengths between atoms, fixed bond angles, etc), and/or fixed values of a reaction coordinate or collective variable as for free energy calculations [22, 16] or model reduction [19, 39]. In computational statistics,  $\xi$  can be some summary statistics and sampling on  $\Sigma$  is relevant in approximate Bayesian computations [36, 27].

Markov chain Monte Carlo (MCMC) method is a general approach to sample probability distributions, which can be used even when the probability densities are known up to a multiplicative constant. A prominent class of methods are Metropolis-Hastings schemes [28, 18]. On  $\mathbb{R}^d$ , MCMC has been extensively studied due to its applications in a wide range of areas [25, 12]. In particular, the Metropolis-adjusted Langevin Algorithm (MALA) [31, 30] (previously introduced in the molecular dynamics literature [32]) and hybrid Monte Carlo (HMC) [8, 29] are among the most popular MCMC methods that have been successfully applied in applications.

MCMC methods that sample probability distributions on submanifolds have also been considered in the literature [6, 23, 37, 24], and have also been implemented in packages [13]. In

particular, the authors in [37] proposed a MCMC algorithm on submanifolds using a reversible Metropolis random walk, which was then extended in [24] to a generalized HMC scheme on submanifolds with non-zero gradient forces in the map used in the proposal step. In contrast to MCMC methods on  $\mathbb{R}^d$ , MCMC methods on submanifolds involve constraints in order to guarantee that the Markov chain stays on the submanifold. As a result, the proposal maps are often nonlinear and are implicitly defined by constraint equations. It has first been noticed in [37] that performing a reversibility check in the MCMC iterations is important in order to guarantee that the Markov chain unbiasedly samples the target probability distribution on the submanifold. In essence, the reversibility check amounts to verifying that the numerical methods started from a new configuration can effectively go back to the previous one, which may not be the case when the projection step finds a different solution to the nonlinear equation under consideration. Let us mention here that an alternative to solving nonlinear equation is to enforce the projection by following the flow of an appropriate ODE, as done in [38].

Based on the previous works [37, 24], we study here MCMC methods to sample probability measures on the level set  $\Sigma$  in (1), defined as

$$\nu(dx) = \frac{1}{Z_\nu} e^{-\beta V(x)} \sigma_\Sigma(dx), \quad (2)$$

where  $\sigma_\Sigma$  is the surface measure on  $\Sigma$  induced by the standard Euclidean scalar product in  $\mathbb{R}^d$ ,  $V : \mathbb{R}^d \rightarrow \mathbb{R}$  is a  $C^1$  potential energy function,  $\beta > 0$  is a parameter (proportional to the inverse temperature in the context of statistical physics), and  $Z_\nu$  is a normalization constant. The first method is a MCMC algorithm in state space (*i.e.* the unknowns are  $x$  only), while the second one is a MCMC algorithm in phase space, where some additional velocity or momentum variable conjugated to the position variable  $x$  is introduced. While the new algorithms share similarities with the ones in [37, 24], the main novelty is that we combine a local property of measure preservation (with a RATTLE scheme to integrate constrained Hamiltonian dynamics), and a global construction of many solutions to propose new algorithms. Allowing for several solutions of the constraint equation can be beneficial both because it can reduce the overall rejection rate, and probably more importantly because it may allow for larger, non-local moves. The algorithms we propose include a generalization of the “reverse projection check” of E. Zappa, M. Holmes-Cerfon and J. Goodman [37] to the situations where multiple projections can be computed. In particular, when the projection algorithm is able to find all the possible projections on the manifold (which is for example possible for algebraic submanifolds), this reverse projection check is not needed anymore and one only needs to count the number of possible projections, see Remarks 3 and 4. We show that the first MCMC algorithm we propose generates a Markov chain in state space that is *reversible* with respect to the target probability distribution, while the second one generates a Markov chain in phase space that is *reversible up to momentum reversal* with respect to the target probability distribution (see Definitions 1–2 in Section 2). In the following, we will simply say that a Markov chain is reversible (possibly up to momentum reversal), when the target probability distribution is clear from the context. The proofs of the consistency of the new algorithms also reveal the connections between the geometric point of view of [37] and the symplectic point of view of [24].

**Outline of the work.** This paper is organized as follows. In Section 2, we introduce the new MCMC algorithms we propose and state the main results about their consistency, whose proofs are postponed to Section 4. We next demonstrate in Section 3 the interest of the new MCMC algorithms on two simple numerical examples. The code used for producing the numerical results in Section 3 is available at <https://github.com/zwpku/Constrained-HMC>.

**Notation and assumptions used throughout this work.** We conclude this section by introducing some useful notation and stating the assumptions we need on the function  $\xi$ . For any  $x \in \mathbb{R}^d$ ,  $\nabla\xi(x)$  denotes the  $d \times k$  matrix whose entries are  $(\nabla\xi(x))_{ij} = \frac{\partial\xi_j}{\partial x_i}(x)$  for  $1 \leq i \leq d$  and  $1 \leq j \leq k$  (i.e. the  $j$ th column of  $\nabla\xi$  is  $\nabla\xi_j$ ), where  $1 \leq k < d$ . The matrix  $I_n \in \mathbb{R}^{n \times n}$  denotes the identity matrix of order  $n$ . The number of elements of a finite set  $A$  is denoted by  $|A|$ . When  $f : \mathcal{M}_1 \rightarrow \mathcal{M}_2$  is a  $C^1$ -differentiable map from an  $m_1$ -dimensional manifold  $\mathcal{M}_1$  to an  $m_2$ -dimensional manifold  $\mathcal{M}_2$ , we denote by  $Df(x) : T_x\mathcal{M}_1 \rightarrow T_{f(x)}\mathcal{M}_2$  the differential of  $f$  at the point  $x \in \mathcal{M}_1$ . When  $\mathcal{M}_1 \subseteq \mathbb{R}^{m_1}$  and  $\mathcal{M}_2$  is embedded in  $\mathbb{R}^m$  with  $m \geq m_2$ , we write  $\nabla f$  for the usual gradient of  $f$ , where  $f$  is viewed as a map  $f : \mathcal{M}_1 \rightarrow \mathbb{R}^m$  between two Euclidean spaces. The notations  $D_x$  and  $\nabla_x$  are used to emphasize that the derivation is performed with respect to the variable  $x$ . We will also use some results in differential topology [2]. When  $m_1 \geq m_2$ , the map  $f$  is a submersion at  $x \in \mathcal{M}_1$  if  $Df(x) : T_x\mathcal{M}_1 \rightarrow T_{f(x)}\mathcal{M}_2$  is onto. In this case,  $x$  is called a regular point and otherwise  $x$  is a critical point. Denote by  $C \subset \mathcal{M}_1$  the set of critical points of  $f$ . A point  $y \in \mathcal{M}_2$  is said to be a regular value if  $f^{-1}(y) \cap C = \emptyset$ . Recall that the regular value theorem states that  $f^{-1}(y)$  is an  $(m_1 - m_2)$ -dimensional submanifold of  $\mathcal{M}_1$ , provided that  $y$  is a regular value and  $f^{-1}(y)$  is non-empty. Sard's theorem asserts that the image  $f(C)$  of  $C$  has zero Lebesgue measure as a subset in  $\mathcal{M}_2$ . Finally, we also introduce a  $C^1$  potential energy  $\bar{V} : \mathbb{R}^d \rightarrow \mathbb{R}$  which can be different from the function  $V$  in (2). Throughout this paper, we make the following assumption.

**Assumption 1.** *Both functions  $V$  and  $\bar{V}$  are  $C^1$ -differentiable. The function  $\xi : \mathbb{R}^d \rightarrow \mathbb{R}^k$  is smooth, and the submanifold  $\Sigma$  is a compact subset of  $\mathbb{R}^d$ . For all  $x \in \Sigma$ , the matrix  $\nabla\xi(x)^T \nabla\xi(x) \in \mathbb{R}^{k \times k}$  is positive definite.*

**Remark 1.** *The assumption that  $\nabla\xi(x)^T \nabla\xi(x)$  is positive definite is equivalent to the assumption that the matrix  $\nabla\xi(x) \in \mathbb{R}^{d \times k}$  has full rank (i.e. rank  $k$ ). This is equivalent to the fact that  $\nabla\xi(x)^T M^{-1} \nabla\xi(x) \in \mathbb{R}^{k \times k}$  is positive definite for any symmetric positive definite matrix  $M \in \mathbb{R}^{d \times d}$ .*

The regular value theorem and Assumption 1 imply that  $\Sigma$  is a  $(d - k)$ -dimensional submanifold of  $\mathbb{R}^d$ .

## 2 Markov chain Monte Carlo algorithms on $\Sigma$ and $T^*\Sigma$

In this section, we introduce two MCMC algorithms sampling the probability measure  $\nu$  on the level set  $\Sigma$ : a first one in the state space  $\Sigma$ , based on the standard MALA method (see Section 2.1); and a second one in the phase space  $T^*\Sigma$ , based on HMC and its generalizations (see Section 2.2). Both algorithms use set-valued proposal maps which encode the numerical projections of an unconstrained move back to the submanifold. Examples of such proposal maps are presented in Section 2.3.

## 2.1 Multiple projection Metropolis-adjusted Langevin algorithm on $\Sigma$

The first algorithm we consider generates a Markov chain on the submanifold  $\Sigma$ . We suppose that Assumption 1 holds. We first introduce in Section 2.1.1 the set-valued proposal map that will be used in the algorithm, the algorithm itself being presented in Section 2.1.2. Finally, we provide a result on the reversibility of this algorithm in Section 2.1.3.

### 2.1.1 Construction of the set-valued map

Let us fix  $x \in \Sigma$ . The objective of this section is to build a map which will be used to propose a move from  $x \in \Sigma$  to another point in  $\Sigma$  in the Metropolis-Hastings algorithm.

**Projection of the unconstrained move.** The modified potential  $\bar{V}$  in Assumption 1 is used to define the drift term in the proposal function; see the discussion after Theorem 1 below for further considerations on the choice of  $V$ . When  $\bar{V} = 0$ , random walk type proposals are recovered, while the standard MALA algorithm corresponds to the choice  $\bar{V} = V$ .

We denote by  $U_x$  a  $d \times (d - k)$  matrix whose  $(d - k)$  column vectors form an orthonormal basis of the tangent space  $T_x \Sigma$ , so that  $U_x^T U_x = I_{d-k} \in \mathbb{R}^{(d-k) \times (d-k)}$ . In view of Assumption 1, we can consider without loss of generality that the map  $x \mapsto U_x$  is chosen so that it is smooth on a neighborhood of  $x$ .

The proposal map increments the position using a velocity in the tangent space  $T_x \Sigma = \{U_x v \mid v \in \mathbb{R}^{d-k}\}$ , adds some drift, and projects back in the direction of  $\nabla \xi(x)$ . This is encoded by the function  $F_x : \mathbb{R}^{d-k} \times \mathbb{R}^k \rightarrow \mathbb{R}^d$  defined as

$$F_x(v, c) = x - \tau \nabla \bar{V}(x) + \sqrt{2\tau} U_x v + \nabla \xi(x) c, \quad v \in \mathbb{R}^{d-k}, \quad c \in \mathbb{R}^k, \quad (3)$$

where  $\tau > 0$  is a fixed timestep, and  $c$  has to be chosen so that  $F_x(v, c) \in \Sigma$ . More precisely, for all  $v \in \mathbb{R}^{d-k}$ , we introduce the set of all possible images by (3):

$$\begin{aligned} \mathcal{F}_x(v) &= \{F_x(v, c) \in \mathbb{R}^k \mid \exists c \in \mathbb{R}^k, \xi(F_x(v, c)) = 0\} \\ &= \left\{ y \in \Sigma \mid \exists c \in \mathbb{R}^k, y = x - \tau \nabla \bar{V}(x) + \sqrt{2\tau} U_x v + \nabla \xi(x) c \right\}, \end{aligned} \quad (4)$$

where  $c$  in (4) plays the role of Lagrange multipliers associated with the constraint  $\xi(F_x(v, c)) = 0$ . It is crucial to note that, given  $y \in \Sigma$ , the vector  $v$  such that  $y = F_x(v, c)$  for some  $c \in \mathbb{R}^k$  (*i.e.*  $y \in \mathcal{F}_x(v)$ ) is uniquely determined (using the facts that  $U_x^T \nabla \xi(x) = 0$  and  $U_x^T U_x = I_{d-k}$ ) by  $v = G_x(y)$ , where  $G_x : \Sigma \rightarrow \mathbb{R}^{d-k}$  is

$$G_x(y) = \frac{1}{\sqrt{2\tau}} U_x^T (y - x + \tau \nabla \bar{V}(x)). \quad (5)$$

**Theoretical results on the projections.** Before introducing the set-valued proposal map which will be used in the algorithms, let us state the following results on the differentiability of the Lagrange multiplier functions, which show that there are various branches for the solutions to the constraint equation, and which motivate Assumption 2 below on the set-valued proposal map. The first result (Proposition 1) focuses on the properties of a single branch, while the

second one states properties of the ensemble of solutions. Not surprisingly, the conditions in Proposition 2 are more restrictive than in Proposition 1, see the discussion in Remark 2 below.

**Proposition 1.** *For any  $x \in \Sigma$ , define the set*

$$C_x = \{y \in \Sigma \mid \det(\nabla\xi(y)^T \nabla\xi(x)) = 0\}. \quad (6)$$

*For all  $y \in \Sigma \setminus C_x$ , denoting by  $v = G_x(y) \in \mathbb{R}^{d-k}$  (so that  $y \in \mathcal{F}_x(v)$ ), the following properties are satisfied:*

1. *There exists a neighborhood  $\mathcal{Q} \subset \Sigma$  of  $y$  such that  $G_x|_{\mathcal{Q}} : \mathcal{Q} \rightarrow G_x(\mathcal{Q}) \subset \mathbb{R}^{d-k}$  is a  $C^1$ -diffeomorphism with  $y = (G_x|_{\mathcal{Q}})^{-1}(v)$  and  $(G_x|_{\mathcal{Q}})^{-1}(\bar{v}) \in \mathcal{F}_x(\bar{v})$  for all  $\bar{v} \in G_x(\mathcal{Q})$ ;*
2. *The Lagrange multiplier function  $c : G_x(\mathcal{Q}) \rightarrow \mathbb{R}^k$ , defined by*

$$c(\bar{v}) = (\nabla\xi(x)^T \nabla\xi(x))^{-1} \nabla\xi(x)^T ((G_x|_{\mathcal{Q}})^{-1}(\bar{v}) - x + \tau \nabla\bar{V}(x)), \quad \bar{v} \in G_x(\mathcal{Q}), \quad (7)$$

*is  $C^1$ -differentiable and satisfies  $y = F_x(v, c(v))$  and  $F_x(\bar{v}, c(\bar{v})) \in \mathcal{F}_x(\bar{v})$ , for all  $\bar{v} \in G_x(\mathcal{Q})$ . Furthermore, any  $C^1$ -differentiable function  $\tilde{c} : \mathcal{O} \rightarrow \mathbb{R}^k$ , where  $\mathcal{O}$  is a neighborhood of  $v$ , such that  $y = F_x(v, \tilde{c}(v))$  and  $F_x(\bar{v}, \tilde{c}(\bar{v})) \in \mathcal{F}_x(\bar{v})$  for all  $\bar{v} \in \mathcal{O}$ , coincides with the function  $c(\cdot)$  in (7) on  $\mathcal{O} \cap G_x(\mathcal{Q})$ .*

Concerning the set  $\mathcal{F}_x(v)$  in (4), we have the following result.

**Proposition 2.** *For any  $x \in \Sigma$ , define the set  $\mathcal{N}_x = G_x(C_x) \subset \mathbb{R}^{d-k}$ , where  $C_x$  is defined in (6). Then the following properties are satisfied:*

1.  *$\mathcal{N}_x$  is a closed set of zero Lebesgue measure in  $\mathbb{R}^{d-k}$ ;*
2. *For all  $v \in \mathbb{R}^{d-k} \setminus \mathcal{N}_x$ , the set  $\mathcal{F}_x(v)$  is finite (possibly empty);*
3. *Consider  $v \in \mathbb{R}^{d-k} \setminus \mathcal{N}_x$  such that  $n = |\mathcal{F}_x(v)| \geq 1$ , and denote by  $\mathcal{F}_x(v) = \{y^{(1)}, y^{(2)}, \dots, y^{(n)}\}$ . Then there exists a neighborhood  $\mathcal{O}$  of  $v$  and  $n$  different  $C^1$ -differentiable Lagrange multiplier functions  $c^{(i)} : \mathcal{O} \rightarrow \mathbb{R}^k$ , which are locally given by (7) by applying Proposition 1 with  $y = y^{(i)}$ , such that  $F_x(v, c^{(i)}(v)) = y^{(i)}$  and*

$$\forall \bar{v} \in \mathcal{O}, \quad \mathcal{F}_x(\bar{v}) = \left\{ F_x(\bar{v}, c^{(1)}(\bar{v})), F_x(\bar{v}, c^{(2)}(\bar{v})), \dots, F_x(\bar{v}, c^{(n)}(\bar{v})) \right\}. \quad (8)$$

*In particular,  $|\mathcal{F}_x(\bar{v})| = n$  for all  $\bar{v} \in \mathcal{O}$ .*

4.  *$\mathbb{R}^{d-k}$  is the disjoint union of the subsets  $\mathcal{N}_x, \mathcal{B}_{x,0}, \mathcal{B}_{x,1}, \dots$ , i.e.  $\mathbb{R}^{d-k} = \left( \bigcup_{i=0}^{+\infty} \mathcal{B}_{x,i} \right) \cup \mathcal{N}_x$ , where the sets*

$$\begin{aligned} \mathcal{B}_{x,0} &= \{v \in \mathbb{R}^{d-k} \mid |\mathcal{F}_x(v)| = 0\}, \\ \mathcal{B}_{x,i} &= \{v \in \mathbb{R}^{d-k} \setminus \mathcal{N}_x \mid |\mathcal{F}_x(v)| = i\}, \quad i = 1, 2, \dots \end{aligned} \quad (9)$$

*are open subsets of  $\mathbb{R}^{d-k}$ .*

The proofs of Propositions 1 and 2 are given in Section 4.1. Note that the condition  $\det(\nabla\xi(y)^T\nabla\xi(x)) = 0$  in (6) is the non-tangential condition considered in [24, Definition 2.1].

**Remark 2.** Note that, on the one hand, the condition  $v \in \mathbb{R}^{d-k} \setminus \mathcal{N}_x$  in Proposition 2 implies that  $y^{(i)} \in \Sigma \setminus C_x$ . On the other hand, in contrast to Proposition 2, Proposition 1 holds for  $y \in \Sigma \setminus C_x$ , even if  $v = G_x(y) \in \mathcal{N}_x$ . The difference comes from the fact that there may be multiple solutions for a given  $v$ , some of which satisfy the non-tangential condition while others do not (see for instance Figure 1, middle picture: the upper point  $y_1$  and the lower point  $y_2$  satisfy the non-tangential condition, but the points on the vertical segment, e.g., the point  $y_3$ , do not). In fact, as shown in Figure 1, the set  $\mathcal{F}_x(v)$  may become quite complicated when  $v \in \mathcal{N}_x$ . In practice, in the algorithm we will present below, the probability to draw a velocity in  $\mathcal{N}_x$  is zero.

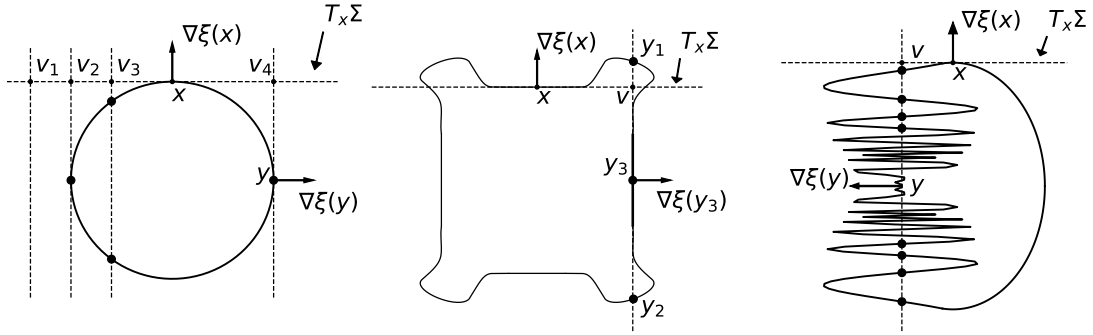


Figure 1: Illustrative examples of the sets  $\mathcal{F}_x(v)$  in (4) and  $\mathcal{N}_x$  in Proposition 2. Left:  $\xi(x) = \frac{1}{2}(x_1^2 + x_2^2 - 1)$  (see Example 1). The set  $\mathcal{F}_x(v)$  has 0, 1, or 2 elements, for  $|v| > 1$ ,  $|v| = 1$ , or  $|v| < 1$ , respectively. The vector  $v_4$  is in  $\mathcal{N}_x$  and  $\nabla\xi^T(y)\nabla\xi(x) = 0$  for  $y \in \mathcal{F}_x(v_4)$ . Middle and right: the set  $\mathcal{F}_x(v)$  may contain an infinite number of elements (countable or not) when  $v \in \mathcal{N}_x$ . The smooth submanifold in the right plot can be constructed using the smooth curve  $x_1 = e^{-1/x_2^2} \sin(1/x_2)$  when  $x_2 \neq 0$ , and  $x_1 = 0$  when  $x_2 = 0$ .

**The set-valued proposal map.** The set-valued proposal map, denoted by  $\Psi_x(v)$ , is a subset of  $\mathcal{F}_x(v)$  which encodes the projections obtained numerically by solving the (nonlinear) constraint equation (see Section 2.3 for concrete examples):

$$\text{Find } c \in \mathbb{R}^k \text{ such that } \xi(F_x(v, c)) = \xi\left(x - \tau\nabla\bar{V}(x) + \sqrt{2\tau}U_x v + \nabla\xi(x)c\right) = 0. \quad (10)$$

The set  $\Psi_x(v)$  is empty if no solutions of (10) are found, and contains more than one elements when multiple solutions can be found. We denote the image of  $\Psi_x$  by  $\text{Im}\Psi_x$ . Note that (5) implies that

$$\forall x \in \Sigma, \quad \forall v, \bar{v} \in \mathbb{R}^{d-k}, \quad v \neq \bar{v} \implies \Psi_x(v) \cap \Psi_x(\bar{v}) = \emptyset. \quad (11)$$

We make the following assumption on the map  $\Psi_x$ .

**Assumption 2.** Fix  $x \in \Sigma$ . The following properties are satisfied:

1. For all  $v \in \mathbb{R}^{d-k}$ ,  $\Psi_x(v)$  contains at most a finite number of elements;
2. The set

$$\mathcal{D} = \{(x, y) \in \Sigma \times \Sigma \mid y \in \text{Im}\Psi_x, x \in \text{Im}\Psi_y\} \quad (12)$$

is a non-empty measurable subset of  $\Sigma \times \Sigma$ ;

3. For all  $v \in \mathbb{R}^{d-k}$  such that  $n = |\Psi_x(v)| \geq 1$ , denote by  $\Psi_x(v) = \{y_1, \dots, y_n\}$  where (upon reordering)  $y_1, \dots, y_m \in \Sigma \setminus C_x$  for some  $m \leq n$ . When  $m \geq 1$ , there exists a neighborhood  $\mathcal{O}$  of  $v$  and  $m$  different  $C^1$ -diffeomorphisms  $\Psi_x^{(j)} : \mathcal{O} \rightarrow \Psi_x^{(j)}(\mathcal{O}) \subset \Sigma$ ,  $1 \leq j \leq m$ , such that  $y_j = \Psi_x^{(j)}(v)$  and  $\Psi_x^{(j)}(\bar{v}) \in \Psi_x(\bar{v})$ , for all  $\bar{v} \in \mathcal{O}$ .

We refer to Section 2.3 for a discussion on set-valued maps satisfying these assumptions.

**Example 1.** Let us give a simple concrete example of a set-valued map  $\Psi_x$ . Consider  $\xi(x) = (x_1^2 + x_2^2 - 1)/2$  for  $x = (x_1, x_2)^T \in \mathbb{R}^2$ . The level set  $\Sigma = \{x \in \mathbb{R}^2 \mid \xi(x) = 0\}$  is the unit circle (see Figure 1, left). Fixing without loss of generality  $x = (0, 1)^T$ , it holds  $\nabla \xi(x) = (0, 1)^T$  so that we can choose  $U_x = (1, 0)^T$ . We set  $\bar{V}(x) \equiv 0$  and  $\tau = 1/2$ . In this case, the constraint equation (10) has 0, 1, or 2 solutions, when  $|v| > 1$ ,  $|v| = 1$ , or  $|v| < 1$ , respectively. The sets in Proposition 1 are then  $C_x = \{(-1, 0)^T, (1, 0)^T\}$  and  $\mathcal{N}_x = \{-1, 1\}$ . In this case, one can define  $\Psi_x(v) = \{(v, \sqrt{1-v^2})^T, (v, -\sqrt{1-v^2})^T\}$ , for  $|v| < 1$  and  $\Psi_x(v) = \emptyset$ , for  $|v| \geq 1$ . For  $|v| < 1$ , the maps  $\Psi_x^{(j)}$  can be taken as  $\Psi_x^{(1)}(\bar{v}) = (\bar{v}, \sqrt{1-\bar{v}^2})^T$ ,  $\Psi_x^{(2)}(\bar{v}) = (\bar{v}, -\sqrt{1-\bar{v}^2})^T$ . They are clearly  $C^1$ -differentiable in  $\{v, |v| < 1\}$ .

### 2.1.2 Presentation of the algorithm

We are now in position to introduce the multiple projection MALA algorithm, see Algorithm 1.

---

#### Algorithm 1 Multiple projection MALA on $\Sigma$

---

- 1: Choose  $x^{(0)} \in \Sigma$  and  $N > 1$ . Set  $i = 0$ .
- 2: **while**  $i < N$  **do**
- 3:   Set  $x = x^{(i)}$ .
- 4:   Randomly draw  $v \in \mathbb{R}^{d-k}$  according to  $v \sim (2\pi\beta^{-1})^{-\frac{d-k}{2}} e^{-\frac{\beta|v|^2}{2}} dv$ .
- 5:   Compute the set  $\Psi_x(v)$  by solving (10). If  $\Psi_x(v) = \emptyset$ , set  $x^{(i+1)} = x$  and go to Step 10.
- 6:   Randomly draw a proposal state  $y \in \Psi_x(v)$  with probability  $\omega(y \mid x, v)$ , and set  $\tilde{x}^{(i+1)} = y$ .
- 7:   Compute  $v'$  as given by (14), and the set  $\Psi_y(v')$ .
- 8:   Check whether  $x \in \Psi_y(v')$ . If this is not true, set  $x^{(i+1)} = x$  and go to Step 10.
- 9:   Draw a random number  $r$  uniformly distributed in  $[0, 1]$ . Set

$$x^{(i+1)} = \begin{cases} \tilde{x}^{(i+1)}, & \text{if } r \leq a(\tilde{x}^{(i+1)} \mid x^{(i)}) \\ x^{(i)}, & \text{otherwise,} \end{cases}$$

with the acceptance probability defined in (17).

- 10:    $i \leftarrow i + 1$ .
  - 11: **end while**
- 

Let us discuss the different steps of one iteration of the algorithm: (i) the choice of a proposed move  $\tilde{x}^{(i+1)}$  starting from a current state  $x = x^{(i)}$ ; (ii) the verification of the reversibility

condition; (iii) the acceptance/rejection of the proposal through a Metropolis-Hastings procedure.

**Choice of proposal.** The proposal state  $\tilde{x}^{(i+1)}$  is constructed as follows:

1. Draw  $v \in \mathbb{R}^{d-k}$  according to the  $(d-k)$ -dimensional Gaussian measure with density

$$(2\pi\beta^{-1})^{-\frac{d-k}{2}} e^{-\frac{\beta|v|^2}{2}} dv, \quad v \in \mathbb{R}^{d-k}. \quad (13)$$

2. Set  $\tilde{x}^{(i+1)} = x$  if  $\Psi_x(v) = \emptyset$ ; otherwise, randomly choose an element  $y \in \Psi_x(v)$  with probability  $\omega(y|x, v)$ , and set  $\tilde{x}^{(i+1)} = y$ .

The probabilities  $(\omega(y|x, v))_{y \in \Psi_x(v)}$  are chosen in  $(0, 1)$  and such that  $\sum_{y \in \Psi_x(v)} \omega(y|x, v) = 1$ .

For instance,  $\omega(\cdot|x, v)$  can be chosen uniformly, *i.e.*  $\omega(y|x, v) = \frac{1}{|\Psi_x(v)|}$  for all  $y \in \Psi_x(v)$ . Alternatively, they can be chosen so that it is more likely to jump to states that are close to (respectively far from) the current state  $x^{(i)}$ , *i.e.*  $\omega(y|x, v) \geq \omega(y'|x, v)$  whenever  $|y - x| \leq |y' - x|$  (respectively  $|y - x| \geq |y' - x|$ ). Note also that the set  $\mathcal{N}_x$  in Proposition 2 has zero measure under the Gaussian measure in (13), since it has zero Lebesgue measure. Therefore, the probability to draw a velocity in  $\mathcal{N}_x$  is zero.

**Reversibility check.** Once the proposal states have been computed using the map  $\Psi_x$ , a reversibility check is in general needed in order to guarantee that the algorithm generates a reversible Markov chain and therefore samples the target distribution  $\nu$  without bias [37]. Specifically, after randomly choosing  $y \in \Psi_x(v)$ , one verifies that  $x \in \Psi_y(v')$  for some  $v' \in \mathbb{R}^{d-k}$ . Note that such an element  $v'$  is uniquely given by

$$v' = G_y(x) = \frac{1}{\sqrt{2\tau}} U_y^T (x - y + \tau \nabla \bar{V}(y)). \quad (14)$$

Therefore, one only needs to check that, after numerically solving for the solutions  $\bar{c}$  of the equation

$$x' = F_y(v', \bar{c}), \quad \xi(x') = 0, \quad (15)$$

one obtains one solution  $\bar{c}$  such that  $x' = x$ .

Note that, with  $v'$  given in (14), we actually have  $x' = x$  in (15) for the choice

$$\bar{c} = [\nabla \xi^T(y) \nabla \xi(y)]^{-1} \nabla \xi^T(y) (x - y + \tau \nabla \bar{V}(y)). \quad (16)$$

In other words, it is guaranteed that  $x \in \mathcal{F}_y(v')$ . The reversibility check thus amounts to verifying that the Lagrange multiplier in (16) is indeed among the possibly many solutions  $\Psi_y(v')$  found by the numerical method used to solve (15) numerically. If it is indeed the case, there is a positive probability to get back to the initial state  $x^{(i)}$  when starting from the proposed state  $\tilde{x}^{(i+1)}$ . A consequence of this discussion is the following important remark.

**Remark 3.** *In the case where the numerical solver is able to find all the solutions to (10), Step 8 in Algorithm 1 (the “reversibility check”) is actually not needed anymore since, by construction,*



$x \in \Psi_y(v')$ .

**Metropolis procedure.** When the reversibility check is successful, *i.e.*  $x \in \Psi_y(v')$ , a Metropolis-Hastings step is performed to either accept or reject the proposal state  $y \in \Psi_x(v)$ , based on the acceptance probability  $a(\tilde{x}^{(i)} | x^{(i)})$ , where

$$a(y | x) = \min \left\{ 1, \frac{\omega(x | y, v')}{\omega(y | x, v)} e^{-\beta[(V(y) + \frac{1}{2}|v'|^2) - (V(x) + \frac{1}{2}|v|^2)]} \right\}, \quad (17)$$

where  $v'$  is defined in (14). In particular, when the state  $y$  is drawn with a uniform probability (*i.e.*, for all  $x \in \Sigma$  and  $v \in \mathbb{R}^{d-k}$ ,  $\omega(y | x, v) = \frac{1}{|\Psi_x(v)|}$  for all  $y \in \Psi_x(v)$ ), the acceptance rate (17) becomes

$$a(y | x) = \min \left\{ 1, \frac{|\Psi_x(v)|}{|\Psi_y(v')|} e^{-\beta[(V(y) + \frac{1}{2}|v'|^2) - (V(x) + \frac{1}{2}|v|^2)]} \right\}.$$

### 2.1.3 Consistency of the algorithm

Let us recall the following definition of the reversibility of Markov chains.

**Definition 1.** A Markov chain on  $\Sigma$  with transition probability kernel  $q(x, dy)$  is reversible with respect to the measure  $\nu(dx)$  if the following equality holds: For any bounded continuous function  $f : \Sigma \times \Sigma \rightarrow \mathbb{R}$ ,

$$\int_{\Sigma \times \Sigma} f(x, y) q(x, dy) \nu(dx) = \int_{\Sigma \times \Sigma} f(y, x) q(x, dy) \nu(dx). \quad (18)$$

One can verify that a Markov chain  $(x^{(i)})_{i \geq 0} \subset \Sigma$  is reversible with respect to  $\nu$  if and only if, for any integer  $n > 0$ , the law of the sequence  $(x^{(0)}, x^{(1)}, \dots, x^{(n)})$  is the same as the law of the sequence  $(x^{(n)}, x^{(n-1)}, \dots, x^{(0)})$ ,  $x^{(0)}$  being distributed according to  $\nu$ . In particular, this implies that  $\nu$  is an invariant measure of the Markov chain.

The following theorem states that Algorithm 1 indeed generates a reversible Markov chain with respect to the measure  $\nu = Z_\nu^{-1} e^{-\beta V(x)} \sigma_\Sigma(dx)$  defined in (2). Its proof is given in Section 4.1.

**Theorem 1.** Under Assumptions 1 and 2, Algorithm 1 generates a Markov chain on  $\Sigma$  which is reversible with respect to the probability measure  $\nu$ . In particular, this Markov chain preserves the probability measure  $\nu$ .

To prove the ergodicity of the Markov chain generated by Algorithm 1, one still needs to verify irreducibility. We refer to [7, 9, 26, 33] for related results in this direction in the unconstrained case, which can be adapted to Markov chains involving constraints as in [15].

As already discussed at the beginning of Section 2.1.1, we have the freedom to choose the function  $\bar{V}$  when defining the set-valued proposal map  $\Psi_x(v)$ . In practice, choosing  $\bar{V}$  as either  $V$  or some simplified (coarse-grained) approximation of  $V$  may be helpful in increasing the acceptance rate in the Metropolis procedure, and therefore allowing for a larger timestep  $\tau$ .

Alternatively, setting  $\bar{V} \equiv 0$ , (10) becomes

$$\text{Find } c \in \mathbb{R}^k \text{ such that } \xi \left( x + \sqrt{2\tau} U_x v + \nabla \xi(x) c \right) = 0. \quad (19)$$

This yields the multiple projection random walk Metropolis-Hastings (RWMH) algorithm on  $\Sigma$ . In this case, assuming furthermore at most one solution of (19) is used (namely  $|\Psi_x(v)| = 0$  or 1), we recover the MCMC algorithm proposed in [37].

## 2.2 Multiple projection Hybrid Monte Carlo on $T^*\Sigma$

The second algorithm we consider generates a Markov chain on an extended configuration space, where a momentum  $p$  conjugated to the position  $x$  is introduced. We first make precise the extended target measure in Section 2.2.1 and then the set-valued proposal function constructed using discretization schemes for constrained Hamiltonian dynamics in Section 2.2.2. The complete algorithm is next presented in Section 2.2.3, while its reversibility properties are stated in Section 2.2.4.

### 2.2.1 Extended target measure

Suppose again that Assumption 1 holds true. Instead of considering  $v$  as coefficients in the tangent space as in (3), we work with momenta  $p$  which belong to the cotangent space. The state of the system is then described by  $(x, p)$ , where, for a given position  $x \in \Sigma$ , the momentum  $p$  belong to  $T_x^*\Sigma$ , the cotangent space of  $\Sigma$  at  $x$ . This cotangent space can be identified with a linear subspace of  $\mathbb{R}^d$ :

$$T_x^*\Sigma = \left\{ p \in \mathbb{R}^d \mid [\nabla \xi(x)]^T M^{-1} p = 0 \in \mathbb{R}^k \right\} \subset \mathbb{R}^d,$$

where  $M \in \mathbb{R}^{d \times d}$  is a constant symmetric positive definite mass matrix. Let us denote by

$$T^*\Sigma = \left\{ (x, p) \in \mathbb{R}^d \times \mathbb{R}^d \mid \xi(x) = 0 \text{ and } [\nabla \xi(x)]^T M^{-1} p = 0 \right\} \subset \mathbb{R}^d \times \mathbb{R}^d$$

the associated cotangent bundle, which can be seen as a submanifold of  $\mathbb{R}^d \times \mathbb{R}^d$ . The phase space Liouville measure on  $T^*\Sigma$  is denoted by  $\sigma_{T^*\Sigma}(dx dp)$ . It can be written in tensorial form as

$$\sigma_{T^*\Sigma}(dx dp) = \sigma_\Sigma^M(dx) \sigma_{T_x^*\Sigma}^{M^{-1}}(dp), \quad (20)$$

where  $\sigma_\Sigma^M(dx)$  is the surface Lebesgue measure on  $\Sigma$  induced by the scalar product  $\langle x, \tilde{x} \rangle_M = x^T M \tilde{x}$  in  $\mathbb{R}^d$ , and  $\sigma_{T_x^*\Sigma}^{M^{-1}}(dp)$  is the Lebesgue measure on  $T_x^*\Sigma$  induced by the scalar product

$$\langle p, \tilde{p} \rangle_{M^{-1}} = p^T M^{-1} \tilde{p} \quad (21)$$

in  $\mathbb{R}^d$ . In particular,  $\sigma_\Sigma^M$  coincides with  $\sigma_\Sigma$  in (2) when  $M = I_d$  is the identity mass matrix. Note that, in contrast with the measures  $\sigma_\Sigma^M(dx)$  and  $\sigma_{T_x^*\Sigma}^{M^{-1}}(dp)$ , the measure  $\sigma_{T^*\Sigma}(dx dp)$  does not depend on the choice of the mass tensor  $M$  (see [22, Proposition 3.40]). For a given  $x \in \Sigma$ , the orthogonal projection  $P_M(x) : \mathbb{R}^d \rightarrow T_x^*\Sigma$  on  $T_x^*\Sigma$  with respect to the scalar product  $\langle \cdot, \cdot \rangle_{M^{-1}}$  is

given by

$$P_M(x) = I_d - \nabla\xi(x)(\nabla\xi^T M^{-1} \nabla\xi)^{-1}(x) \nabla\xi(x)^T M^{-1}.$$

It is well-defined on  $\Sigma$  thanks to Assumption 1 (see Remark 1).

The target measure to sample is

$$\mu(dx dp) = \frac{1}{Z_\mu} e^{-\beta H(x,p)} \sigma_{T^*\Sigma}(dx dp), \quad (22)$$

where  $H$  is the Hamiltonian

$$H(x,p) = V(x) + \frac{1}{2} p^T M^{-1} p.$$

Note that, thanks to the tensorization property (20) and the separability of the Hamiltonian function,

$$\mu(dx dp) = \nu_M(dx) \kappa_x(dp), \quad (23)$$

where (see (3.25) in [22, Section 3.2.1.3])

$$\nu_M(dx) = (\det M)^{1/2} [\det(\nabla\xi(x)^T M^{-1} \nabla\xi(x))]^{1/2} [\det(\nabla\xi(x)^T \nabla\xi(x))]^{-1/2} \nu(dx), \quad (24)$$

with  $\nu$  defined in (2), while  $\kappa_x$  is a Gaussian measure on  $T_x^*\Sigma$ :

$$\kappa_x(dp) = (2\pi\beta^{-1})^{-\frac{d-k}{2}} \exp\left(-\frac{\beta p^T M^{-1} p}{2}\right) \sigma_{T_x^*\Sigma}^{M^{-1}}(dp). \quad (25)$$

In particular, the marginal of  $\mu$  in the variable  $x$  is  $\nu_M$ , which can be easily related to  $\nu$  by (24) using some importance sampling weight or by modifying the potential function  $V$ . It coincides in fact with  $\nu$  when  $M = I_d$  is the identity mass matrix.

For further notice, let us introduce the momentum reversal map  $\mathcal{R}$ , which is an involution:

$$\mathcal{R}(x,p) = (x, -p), \quad \forall (x,p) \in T^*\Sigma. \quad (26)$$

Notice that  $\mu(dx dp)$  is invariant under  $\mathcal{R}$ .

### 2.2.2 Construction of the set-valued map

Let us fix  $(x,p) \in T^*\Sigma$ . The objective of this section is to build a map which will be used to propose a move from  $(x,p) \in T^*\Sigma$  to another point in  $T^*\Sigma$  in the Metropolis-Hastings algorithm.

**Projection of the unconstrained move: RATTLE.** Given a timestep  $\tau > 0$  and a potential energy function  $\bar{V}$  (as in Section 2.1.1, see the discussion on the choices of the potential  $\bar{V}$ )

after Theorem 1), the multiple projection HMC algorithm uses the following unconstrained move:

$$\begin{cases} p^{1/2} = p - \frac{\tau}{2} \nabla \bar{V}(x) + \nabla \xi(x) \lambda_x, & (27a) \\ x^1 = x + \tau M^{-1} p^{1/2}, & \\ \xi(x^1) = 0, & (27b) \\ p^1 = p^{1/2} - \frac{\tau}{2} \nabla \bar{V}(x^1) + \nabla \xi(x^1) \lambda_p, & \\ \nabla \xi(x^1)^T M^{-1} p^1 = 0, & (27c) \\ p^{1,-} = -p^1, & (27d) \end{cases}$$

where  $\lambda_x, \lambda_p \in \mathbb{R}^k$  are Lagrange multiplier functions determined by the constraints (27b) and (27c), respectively. Note that the scheme from  $(x, p)$  to  $(x^1, p^{1,-})$  combines the one-step RATTLE scheme [14] (*i.e.*, (27a)–(27c)) with a momentum reversal step in (27d). For this reason, we will call the scheme (27a)–(27d) “one-step RATTLE with momentum reversal”. Let us recall the main properties of the above scheme.

First, for any  $(x, p) \in T^*\Sigma$  and  $(c_x, c_p) \in \mathbb{R}^k \times \mathbb{R}^k$ , we denote by  $F : T^*\Sigma \times \mathbb{R}^k \times \mathbb{R}^k \rightarrow \mathbb{R}^d \times \mathbb{R}^d$  the map defined by

$$\begin{aligned} F(x, p, c_x, c_p) &= (\bar{x}, \bar{p}^-), \quad \text{where} \\ \bar{x} &= x + \tau M^{-1} p - \frac{\tau^2}{2} M^{-1} \nabla \bar{V}(x) + \tau M^{-1} \nabla \xi(x) c_x, \\ \bar{p} &= p - \frac{\tau}{2} (\nabla \bar{V}(x) + \nabla \bar{V}(\bar{x})) + \nabla \xi(x) c_x + \nabla \xi(\bar{x}) c_p, \\ \bar{p}^- &= -\bar{p}. \end{aligned} \quad (28)$$

Note that, by eliminating  $p^{1/2}$  and using the map  $F$  in (28), we can write the one-step RATTLE with momentum reversal from  $(x, p)$  to  $(x^1, p^{1,-})$  as

$$\begin{cases} (x^1, p^{1,-}) = F(x, p, \lambda_x, \lambda_p), \\ \xi(x^1) = 0, \\ \nabla \xi(x^1)^T M^{-1} p^{1,-} = 0. \end{cases} \quad (29)$$

Once  $\lambda_x$  (and therefore  $x^1$ ) is known, the Lagrange multiplier  $\lambda_p$  (and therefore  $p^{1,-}$ ) is uniquely defined and can actually be analytically computed by enforcing the projection of the momenta with  $P_M$ :

$$\begin{aligned} \lambda_p &= - [\nabla \xi(x^1)^T M^{-1} \nabla \xi(x^1)]^{-1} \left[ \nabla \xi(x^1)^T M^{-1} \left( p - \frac{\tau}{2} (\nabla \bar{V}(x) + \nabla \bar{V}(x^1)) + \nabla \xi(x) \lambda_x \right) \right], \\ p^{1,-} &= - P_M(x^1) \left( p - \frac{\tau}{2} (\nabla \bar{V}(x) + \nabla \bar{V}(x^1)) + \nabla \xi(x) \lambda_x \right). \end{aligned} \quad (30)$$

Therefore, the main task in finding  $x^1, p^{1,-}$  is to solve the constraint equation (27b) for  $\lambda_x$ .

Consider next a matrix  $U_{M,x} \in \mathbb{R}^{d \times (d-k)}$  whose columns form an orthonormal basis of  $T_x^*\Sigma$  with respect to  $\langle \cdot, \cdot \rangle_{M^{-1}}$ , *i.e.*  $U_{M,x}^T M^{-1} U_{M,x} = I_{d-k}$  and  $\nabla \xi(x)^T M^{-1} U_{M,x} = 0$ . For a given point  $x$ , the map  $x \mapsto U_{M,x}$  can be assumed to be smooth on a neighborhood of  $x$ . It is crucial to realize that for given configurations  $x \in \Sigma$  and  $x^1 \in \Sigma$ , the vector  $p \in T_x^*\Sigma$  such that the one-step

RATTLE with momentum reversal maps to  $(x^1, p^{1,-})$  for some  $p^{1,-}$  is uniquely determined by  $p = G_{M,x}(x^1)$ , where  $G_{M,x} : \Sigma \rightarrow T_x^*\Sigma$  is defined as

$$\begin{aligned} G_{M,x}(x^1) &= \frac{1}{\tau} U_{M,x} U_{M,x}^T \left( x^1 - x + \frac{\tau^2}{2} M^{-1} \nabla \bar{V}(x) \right) \\ &= \frac{1}{\tau} P_M(x) M \left( x^1 - x + \frac{\tau^2}{2} M^{-1} \nabla \bar{V}(x) \right). \end{aligned} \quad (31)$$

Clearly, the map  $G_{M,x}$  does not depend on the choice of the matrix  $U_{M,x}$ .

Let us call  $(\lambda_x, \lambda_p)$  an *admissible pair of Lagrange multipliers* from  $(x, p)$  to  $(x^1, p^{1,-})$  if the constraint equations (27b) and (27c) are satisfied. The one-step RATTLE scheme with momentum reversal has the following time-reversal symmetry.

**Lemma 1.** *Suppose that Assumption 1 is satisfied. Consider two states  $(x, p), (x^1, p^{1,-}) \in T^*\Sigma$  and suppose that  $(\lambda_x, \lambda_p)$  is an admissible pair of Lagrange multipliers from  $(x, p)$  to  $(x^1, p^{1,-})$ . Then,*

1.  $(\lambda_p, \lambda_x)$  is an admissible pair of Lagrange multipliers from  $(x^1, p^{1,-})$  to  $(x, p)$ ;
2. Suppose that  $(\lambda_{\bar{x}}, \lambda_{\bar{p}})$  is an admissible pair of Lagrange multipliers from  $(x^1, p^{1,-})$  to  $(\bar{x}, \bar{p})$  such that  $\bar{x} = x$ . Then,  $(\lambda_{\bar{x}}, \lambda_{\bar{p}}) = (\lambda_p, \lambda_x)$  and  $\bar{p} = p$ .

The first property is standard and expresses some form of symmetry (see for instance [14, Section VII.1.4]). The second expresses some rigidity in the choice of the Lagrange multipliers and shows that genuinely different choices of Lagrange multipliers necessarily correspond to a failure in the time-reversal symmetry of the algorithm; see the proof of [24, Lemma 3.2].

**Theoretical results on the projections.** For  $z = (x, p) \in T^*\Sigma$ , we introduce the set

$$\mathcal{F}(z) = \left\{ (x^1, p^{1,-}) \in T^*\Sigma \mid \exists (\lambda_x, \lambda_p) \in \mathbb{R}^k \times \mathbb{R}^k, (x^1, p^{1,-}) = F(z, \lambda_x, \lambda_p), \right. \\ \left. \text{such that } \xi(x^1) = 0 \text{ and } \nabla \xi(x^1)^T M^{-1} p^{1,-} = 0 \right\}, \quad (32)$$

where  $F$  is the map defined in (28). In other words,  $\mathcal{F}(z)$  contains all the possible outcomes of the one-step RATTLE with momentum reversal starting from  $z$ .

Similarly to Propositions 1 and 2, we have the following results on the differentiability of the Lagrange multiplier functions, as well as on the set  $\mathcal{F}(z)$ . Their proofs are given in Section 4.2.

**Proposition 3.** *Define the set  $C_{M,x}$  as*

$$C_{M,x} = \{ y \in \Sigma \mid \det(\nabla \xi(y)^T M^{-1} \nabla \xi(x)) = 0 \}, \quad x \in \Sigma. \quad (33)$$

*For all  $z = (x, p), z' = (x^1, p^{1,-}) \in T^*\Sigma$  such that  $z' \in \mathcal{F}(z)$  and  $x^1 \in \Sigma \setminus C_{M,x}$ , the following properties are satisfied:*

1. *There exists a neighborhood  $\mathcal{O} \subset T^*\Sigma$  of  $z$  and a  $C^1$ -differentiable function  $\Upsilon_1 : \mathcal{O} \rightarrow \Sigma$  such that  $x^1 = \Upsilon_1(z)$  and  $G_{M,\bar{x}}(\Upsilon_1(\bar{z})) = \bar{p}$  for all  $\bar{z} = (\bar{x}, \bar{p}) \in \mathcal{O}$ . Moreover, this map  $\Upsilon_1$  is unique in the sense that any  $C^1$ -differentiable map  $\tilde{\Upsilon}_1 : \mathcal{O}' \rightarrow \Sigma$ , where  $\mathcal{O}' \subset T^*\Sigma$  is*

a neighborhood of  $z$ , such that  $x^1 = \tilde{\Upsilon}_1(z)$  and  $G_{M,\bar{x}}(\tilde{\Upsilon}_1(\bar{z})) = \bar{p}$  for all  $\bar{z} = (\bar{x}, \bar{p}) \in \mathcal{O}'$ , coincides with  $\Upsilon_1$  on  $\mathcal{O} \cap \mathcal{O}'$ ;

2. Recall the function  $F$  in (28) and the map  $\Upsilon_1 : \mathcal{O} \rightarrow \Sigma$  introduced in the previous item. The Lagrange multiplier functions

$$\begin{aligned} \lambda_x(\bar{z}) &= \frac{1}{\tau} [(\nabla \xi^T M^{-1} \nabla \xi)(\bar{x})]^{-1} \nabla \xi(\bar{x})^T \left[ \Upsilon_1(\bar{z}) - \bar{x} - \tau M^{-1} \bar{p} + \frac{\tau^2}{2} M^{-1} \nabla \bar{V}(\bar{x}) \right], \\ \lambda_p(\bar{z}) &= - [(\nabla \xi^T M^{-1} \nabla \xi)(\Upsilon_1(\bar{z}))]^{-1} \\ &\quad \times \left[ \nabla \xi(\Upsilon_1(\bar{z}))^T M^{-1} \left( \bar{p} - \frac{\tau}{2} (\nabla \bar{V}(\bar{x}) + \nabla \bar{V}(\Upsilon_1(\bar{z}))) + \nabla \xi(\bar{x}) \lambda_x(\bar{z}) \right) \right], \end{aligned} \quad (34)$$

where  $\bar{z} = (\bar{x}, \bar{p}) \in \mathcal{O}$ , are  $C^1$ -differentiable on  $\mathcal{O}$  and such that  $z' = F(z, \lambda_x(z), \lambda_p(z))$  and  $F(\bar{z}, \lambda_x(\bar{z}), \lambda_p(\bar{z})) \in \mathcal{F}(\bar{z})$  for all  $\bar{z} \in \mathcal{O}$ . Furthermore, any  $C^1$ -differentiable functions  $\tilde{\lambda}_x, \tilde{\lambda}_p : \mathcal{O}' \rightarrow \mathbb{R}^k$ , where  $\mathcal{O}'$  is a neighborhood of  $z$  such that  $z' = F(z, \tilde{\lambda}_x(z), \tilde{\lambda}_p(z))$  and  $F(\bar{z}, \tilde{\lambda}_x(\bar{z}), \tilde{\lambda}_p(\bar{z})) \in \mathcal{F}(\bar{z})$  for all  $\bar{z} \in \mathcal{O}'$ , coincide with the functions in (34) on  $\mathcal{O} \cap \mathcal{O}'$ ;

3. There exists a neighborhood  $\mathcal{O} \subset T^*\Sigma$  of  $z$  such that the map  $\Upsilon := F(\cdot, \lambda_x(\cdot), \lambda_p(\cdot)) : \mathcal{O} \rightarrow \Upsilon(\mathcal{O}) \subset T^*\Sigma$  (with  $F$  defined in (28) and the Lagrange multiplier functions  $\lambda_x(\cdot), \lambda_p(\cdot)$  given in (34)) is a  $C^1$ -diffeomorphism on  $\mathcal{O}$  which satisfies  $\Upsilon(z) = z'$  and  $|\det D\Upsilon| \equiv 1$  on  $\mathcal{O}$ .

**Proposition 4.** Define the set  $\mathcal{N} = \{(x, p) \in T^*\Sigma \mid x \in \Sigma, p \in G_{M,x}(C_{M,x})\}$ , where  $G_{M,x}$  is the map in (31) and the set  $C_{M,x}$  is defined in (33). The following properties are satisfied:

1.  $\mathcal{N} \subset T^*\Sigma$  is a closed set of zero Lebesgue measure, and can be defined equivalently as

$$\mathcal{N} = \left\{ (x, p) \in T^*\Sigma \mid \exists z' = (x^1, p^{1,-}) \in \mathcal{F}(x, p), \det(\nabla \xi(x^1)^T M^{-1} \nabla \xi(x)) = 0 \right\}; \quad (35)$$

2. For all  $z \in T^*\Sigma \setminus \mathcal{N}$ , the set  $\mathcal{F}(z)$  contains at most a finite number of elements;
3. For  $z \in T^*\Sigma \setminus \mathcal{N}$ , let  $n = |\mathcal{F}(z)|$  and denote by  $\mathcal{F}(z) = \{z^{(1)}, z^{(2)}, \dots, z^{(n)}\}$ . When  $n \geq 1$ , there exists a neighborhood  $\mathcal{O}$  of  $z$ , as well as  $n$  pairs of  $C^1$ -differentiable functions  $\lambda_x^{(i)}, \lambda_p^{(i)} : \mathcal{O} \rightarrow \mathbb{R}^k$ , which are locally given by (34) in Proposition 3 with  $z' = z^{(i)}$ , such that  $z^{(i)} = F(z, \lambda_x^{(i)}(z), \lambda_p^{(i)}(z)) \in T^*\Sigma$  for any  $1 \leq i \leq n$  and, for all  $\bar{z} \in \mathcal{O}$ ,

$$\mathcal{F}(\bar{z}) = \left\{ F(\bar{z}, \lambda_x^{(1)}(\bar{z}), \lambda_p^{(1)}(\bar{z})), F(\bar{z}, \lambda_x^{(2)}(\bar{z}), \lambda_p^{(2)}(\bar{z})), \dots, F(\bar{z}, \lambda_x^{(n)}(\bar{z}), \lambda_p^{(n)}(\bar{z})) \right\}.$$

In particular,  $|\mathcal{F}(\bar{z})| = n$  for all  $\bar{z} \in \mathcal{O}$ .

4.  $T^*\Sigma$  is the disjoint union of the subsets  $\mathcal{N}, \mathcal{B}_0, \mathcal{B}_1, \dots$ , i.e.  $T^*\Sigma = \left( \bigcup_{i=0}^{+\infty} \mathcal{B}_i \right) \cup \mathcal{N}$ , where the sets

$$\begin{aligned} \mathcal{B}_0 &= \left\{ z \in T^*\Sigma \mid |\mathcal{F}(z)| = 0 \right\}, \\ \mathcal{B}_i &= \left\{ z \in T^*\Sigma \setminus \mathcal{N} \mid |\mathcal{F}(z)| = i \right\}, \quad i = 1, 2, \dots \end{aligned} \quad (36)$$

are open subsets of  $T^*\Sigma$ .

Let us point out that there is some type of symmetry in Proposition 3 in the condition on the two states  $z = (x, p)$ ,  $z' = (x^1, p^{1,-}) \in T^*\Sigma$ , in the sense that  $z' \in \mathcal{F}(z)$ ,  $x^1 \in \Sigma \setminus C_{M,x}$  if and only if  $z \in \mathcal{F}(z')$ ,  $x \in \Sigma \setminus C_{M,x^1}$ , which can be easily seen from Lemma 1 and the definition of the set  $C_{M,x}$  in (33). Moreover, let  $\Upsilon : \mathcal{O} \rightarrow \Upsilon(\mathcal{O})$  with  $\mathcal{O}$  a neighborhood of  $z$ , and  $\tilde{\Upsilon} : \tilde{\mathcal{O}} \rightarrow \tilde{\Upsilon}(\tilde{\mathcal{O}})$  with  $\tilde{\mathcal{O}}$  a neighborhood of  $z'$  be the  $C^1$ -diffeomorphisms considered in the third item of Proposition 3 for  $z, z'$  respectively. Then, by possibly shrinking the neighborhoods (still denoted by  $\mathcal{O}$  and  $\tilde{\mathcal{O}}$ ), Lemma 1 actually implies that  $\tilde{\Upsilon} \circ \Upsilon = \text{id}$  on  $\mathcal{O}$  and  $\Upsilon \circ \tilde{\Upsilon} = \text{id}$  on  $\tilde{\mathcal{O}}$ .

Let us comment on the differences between Propositions 3 and 4, with a discussion similar to the one in Remark 2. On the one hand, the condition  $z = (x, p) \in T^*\Sigma \setminus \mathcal{N}$  in Proposition 4 implies  $x^1 \in \Sigma \setminus C_{M,x}$  for all  $z' = (x^1, p^{1,-}) \in \mathcal{F}(z)$ . On the other hand, in contrast to Proposition 4, Proposition 3 also holds for  $z \in \mathcal{N}$ , as long as  $x^1 \in \Sigma \setminus C_{M,x}$ . Again, the set  $C_{M,x}$  is related to the non-tangential condition of the previous work [24, Definition 2.1]. We also point out that, since  $\mathcal{N}$  has zero Lebesgue measure in  $T^*\Sigma$ , it has zero probability measure under  $\mu$ .

**The set-valued proposal map.** We are now in position to introduce the set-valued proposal map. For  $z = (x, p) \in T^*\Sigma$ , the set-valued proposal map  $\Phi(z)$  is a subset of  $\mathcal{F}(z)$  which contain the projection points obtained by numerically computing the outcomes of the one-step RATTLE scheme with momentum reversal. In other words,  $\Phi(z)$  contains a state  $(x^1, p^{1,-}) \in \mathcal{F}(z)$  if  $(x^1, p^{1,-})$  is obtained numerically by solving for the Lagrange multipliers  $\lambda_x$  and  $\lambda_p$  from (27b)–(27c); *i.e.*  $\Phi(z)$  is a solution of (27b)–(27c) starting from  $z$ . Depending on the number of numerical solutions of (27b)–(27c) for a given  $z = (x, p)$ , the set  $\Phi(z)$  can either be empty or contain multiple states.

Denote by  $\Pi : T^*\Sigma \rightarrow \Sigma$  the projection map

$$\Pi(z) = x, \quad \forall z = (x, p) \in T^*\Sigma. \quad (37)$$

We make the following assumption on the map  $\Phi$ .

**Assumption 3.** *The following properties are satisfied by the map  $\Phi$ :*

1. *For all  $z \in T^*\Sigma$ , the set  $\Phi(z)$  contains at most a finite number of elements;*
2. *The set*

$$\mathcal{D}_\Phi = \left\{ (z, z') \in T^*\Sigma \times T^*\Sigma \mid z' \in \Phi(z) \text{ and } z \in \Phi(z') \right\} \quad (38)$$

*is a non-empty measurable subset of  $T^*\Sigma \times T^*\Sigma$ .*

3. *For all  $z = (x, p) \in T^*\Sigma$  such that  $|\Phi(z)| = n \geq 1$ , denote by  $\Phi(z) = \{z_1, \dots, z_n\}$  with (upon reordering)  $\{z' \in \Phi(z) \mid \Pi(z') \notin C_{M, \Pi(z)}\} = \{z_1, \dots, z_m\}$  where  $m \leq |\Phi(z)|$ . When  $m \geq 1$ , there exists a neighborhood  $\mathcal{O}$  of  $z$ , as well as  $m$  different  $C^1$ -diffeomorphisms  $\Phi^{(j)} : \mathcal{O} \rightarrow \Phi^{(j)}(\mathcal{O}) \subset T^*\Sigma$ ,  $1 \leq j \leq m$ , such that  $z_j = \Phi^{(j)}(z)$  and  $\Phi^{(j)}(\bar{z}) \in \Phi(\bar{z})$  for any  $1 \leq j \leq m$  and  $\bar{z} \in \mathcal{O}$ .*

We refer to Section 2.3 for a discussion on set-valued maps satisfying these assumptions.

### 2.2.3 Presentation of the algorithm

The multiple projection Hybrid Monte Carlo algorithm is given in Algorithm 2 below. It reduces to the algorithm studied in [24] when the proposal is a singled-valued map obtained by computing a single solution of the constraint equations (27b)–(27c) (namely  $|\Phi(z)| = 0$  or 1, where  $\Phi$  is the proposal map introduced in the previous section). Notice also that Algorithm 2 with  $M$  is the identity matrix and  $\alpha = 0$  in (39) below reduces to Algorithm 1.

---

#### Algorithm 2 Multiple projection HMC on $\Sigma$

---

- 1: Choose  $z^{(0)} \in T^*\Sigma$  and  $N > 1$ . Set  $i = 0$ .
- 2: **while**  $i < N$  **do**
- 3:   Update the momenta of the current state  $z^{(i)}$  according to (39), and denote the new state by  $z^{(i+\frac{1}{4})} = z = (x, p)$ .
- 4:   Compute the set  $\Phi(z)$ . If  $\Phi(z) = \emptyset$ , set  $z^{(i+\frac{2}{4})} = z$  and go to Step 9.
- 5:   Randomly choose an element  $z' \in \Phi(z)$  with probability  $\omega(z' | z)$ .
- 6:   Compute the set  $\Phi(z')$ .
- 7:   Check whether  $z \in \Phi(z')$  is true. If this is not true, set  $z^{(i+\frac{2}{4})} = z$  and go to Step 9.
- 8:   Draw a uniformly distributed random number  $r \in [0, 1]$ . Set

$$z^{(i+\frac{2}{4})} = \begin{cases} z' & \text{if } r \leq a(z' | z), \\ z & \text{otherwise,} \end{cases}$$

with the acceptance probability  $a(z' | z)$  defined in (40).

- 9:   Set  $z^{(i+\frac{3}{4})} = \mathcal{R}(z^{(i+\frac{2}{4})})$ .
  - 10:   Update the momenta of the state  $z^{(i+\frac{3}{4})}$  according to (39), and denote the new state by  $z^{(i+1)}$ .
  - 11:    $i \leftarrow i + 1$ .
  - 12: **end while**
- 

Let us now discuss the different algorithmic steps of the multiple projection Hybrid Monte Carlo algorithm.

**Momentum update.** Given the current state  $z = (x, p) \in T^*\Sigma$ , the momentum is updated according to

$$p \leftarrow \alpha p + \sqrt{\frac{1 - \alpha^2}{\beta}} \eta, \quad (39)$$

for some parameter  $|\alpha| < 1$ , where  $\eta$  is a Gaussian random variable in the cotangent space  $T_x^*\Sigma$  with identity covariance with respect to the weighted inner product  $\langle \cdot, \cdot \rangle_{M^{-1}}$ . In practice,  $\eta$  can be obtained from  $\eta = P_M(x)v$ , where  $v$  is a Gaussian random variable on  $\mathbb{R}^d$  with covariance matrix  $M$ , or from  $\eta = \sum_{i=1}^{d-k} w_i e_i$ , where  $(e_1, e_2, \dots, e_{d-k})$  is a basis of  $T_x^*\Sigma$  orthonormal for the scalar product  $\langle \cdot, \cdot \rangle_{M^{-1}}$ , and  $w_i \in \mathbb{R}$  for  $1 \leq i \leq d - k$  are independent and identically distributed (i.i.d) standard Gaussian random variables on  $\mathbb{R}$ . Note also that the update rule (39) could be generalized to matrix-valued  $\alpha$ . Notice that the momentum update is applied both at the beginning and at the end of one iteration of the multiple projection Hybrid Monte Carlo algorithm (see Algorithm 2).



**Choice of proposal.** Remember the set-valued map  $\Phi$  introduced in the previous section. Once  $\Phi(z)$  is available and non-empty (namely  $|\Phi(z)| \geq 1$ ), one randomly chooses an element  $z' = (x^1, p^{1,-}) \in \Phi(z)$  with probability  $\omega(z' | z)$ , and takes it as the proposal state. As in Section 2.1.2, the probabilities  $\omega(\cdot | z)$  are chosen real numbers in  $(0, 1)$  which satisfy, for all  $z \in T^*\Sigma$ ,  $\sum_{z' \in \Phi(z)} \omega(z' | z) = 1$ . They can be chosen uniformly (*i.e.*  $\omega(z' | z) = 1/|\Phi(z)|$ ), or in a way such that it is more likely to jump to states  $x^1$  that are close to, or on the contrary far from, the current state  $x$ .

**Reversibility check.** Similarly to Algorithm 1, a reversibility check step is in general needed in the MCMC algorithm [24]. Specifically, after the proposal state  $(x^1, p^{1,-})$  is chosen, one needs to verify that  $(x, p) \in \Phi(x^1, p^{1,-})$ . For this purpose, one computes  $\Phi(x^1, p^{1,-})$  by solving the constraint equations (27b)–(27c) and checks whether  $(x, p)$  belongs to  $\Phi(x^1, p^{1,-})$ . Note that the second claim in Lemma 1 implies that it is in fact sufficient for the reversibility check step to verify that the positions are the same (as already pointed out in [24, Section 3.1]).

Lemma 1 implies that the one-step RATTLE scheme with momentum reversal is indeed able to map the state  $(x^1, p^{1,-})$  to  $(x, p)$  with the pair of Lagrange multipliers  $(\lambda_p, \lambda_x)$ , *i.e.*  $(x, p) \in \mathcal{F}(x^1, p^{1,-})$ . This means that  $(x, p) \in \Phi(x^1, p^{1,-})$  as long as the pair  $(\lambda_p, \lambda_x)$  is indeed found as a solution of the constraint equations (27b)–(27c) when  $\Phi(x^1, p^{1,-})$  is computed numerically. As a consequence, one has the following remark, as in Section 2.1.2 (see Remark 3).

**Remark 4.** *In the case where the numerical solver is able to find all the solutions to (27b)–(27c), the “reversibility check” performed in Step 7 of Algorithm 2 is actually not needed. More generally, the reversibility check step will not lead to frequent rejections when one is able to compute almost all the solutions of (27b)–(27c). This is clearly an advantage compared to the algorithms in [37, 24], since it yields to a larger acceptance rate.*

**Metropolis procedure.** When the reversibility check step is successful, *i.e.*  $z = (x, p) \in \Phi(x^1, p^{1,-})$ , a Metropolis-Hastings step is performed to decide either to accept or to reject the proposal state  $z' = (x^1, p^{1,-})$ , based on the acceptance ratio

$$a(z' | z) = \min \left\{ 1, \frac{\omega(z | z')}{\omega(z' | z)} e^{-\beta(H(z') - H(z))} \right\}. \quad (40)$$

In particular, when the elements  $z'$  are drawn with uniform probabilities, *i.e.*,  $\omega(z' | z) = \frac{1}{|\Phi(z)|}$  for all  $z' \in \Phi(z)$ , (40) simplifies as

$$a(z' | z) = \min \left\{ 1, \frac{|\Phi(z)|}{|\Phi(z')|} e^{-\beta(H(z') - H(z))} \right\}.$$

## 2.2.4 Consistency of the algorithm

Recall that  $\mathcal{R}(x, p) = (x, -p)$  is the momentum reversal map defined in (26), and that  $\mu$  is invariant by  $\mathcal{R}$ . Let us introduce the following definition of reversibility up to momentum reversal. It is equivalent to the “modified detailed balance” considered in [10, 11] for example.

**Definition 2.** *A Markov chain on  $T^*\Sigma$  with transition probability kernel  $q(z, dz')$  is reversible up to momentum reversal with respect to the probability distribution  $\mu$  if and only if the following*

equality holds: For any bounded continuous function  $f : T^*\Sigma \times T^*\Sigma \rightarrow \mathbb{R}$ ,

$$\int_{T^*\Sigma \times T^*\Sigma} f(z, z') q(z, dz') \mu(dz) = \int_{T^*\Sigma \times T^*\Sigma} f(\mathcal{R}(z'), \mathcal{R}(z)) q(z, dz') \mu(dz). \quad (41)$$

Similarly to Definition 1, one can verify that a Markov chain  $(z^{(i)})_{i \geq 0}$  on  $T^*\Sigma$  is reversible up to momentum reversal with respect to  $\mu$  if and only if, for any integer  $n > 0$ , the law of the sequence  $(z^{(0)}, z^{(1)}, \dots, z^{(n)})$  is the same as the law of the sequence  $(\mathcal{R}(z^{(n)}), \mathcal{R}(z^{(n-1)}), \dots, \mathcal{R}(z^{(0)}))$ ,  $z^{(0)}$  being distributed according to  $\mu$ . In particular, by considering  $f(z, z') = f(z')$  in (41) and using the fact that  $\mu$  is invariant under  $\mathcal{R}$ ,  $\mu$  is an invariant measure if the Markov chain is reversible up to momentum reversal. A simple connection between the reversibility up to momentum reversal of Definition 2 and the reversibility of Definition 1 is the following:

**Lemma 2.** *Let us consider a Markov chain  $\mathcal{C}$  on  $T^*\Sigma$  with transition probability kernel  $q(z, dz')$  and let  $\tilde{\mathcal{C}}$  be the Markov chain on  $T^*\Sigma$  obtained by composing a transition according to  $q$  with a momentum reversal: starting from  $z$ , the new state is  $\mathcal{R}(z')$  where  $z' \sim q(z, dz')$ . Then,  $\mathcal{C}$  is reversible with respect to  $\mu$  if and only if  $\tilde{\mathcal{C}}$  is reversible up to momentum reversal with respect to  $\mu$ .*

We have the following result on the Markov chain generated by Algorithm 2.

**Theorem 2.** *Under Assumptions 1 and 3, Algorithm 2 generates a Markov chain on  $T^*\Sigma$  that is reversible up to momentum reversal with respect to  $\mu$ . In particular, it preserves the probability measure  $\mu$  in (22).*

The proofs of Lemma 2 and Theorem 2 are provided in Section 4.2.

**Remark 5.** *The proof of Theorem 2 consists in checking that the probability measure  $\mu$  is preserved by each of the transitions  $x^{(i)} \rightarrow x^{(i+\frac{1}{4})}$  (Step 3: momentum refreshment),  $x^{(i+\frac{1}{4})} \rightarrow x^{(i+\frac{2}{4})}$  (Steps 4-8: metropolized RATTLE with momentum reversal),  $x^{(i+\frac{2}{4})} \rightarrow x^{(i+\frac{3}{4})}$  (Step 9: momentum reversal), and  $x^{(i+\frac{3}{4})} \rightarrow x^{(i+1)}$  (Step 10: momentum refreshment, which is exactly the same as Step 3). Thus an algorithm which combines any the three above steps (momentum refreshment, metropolized RATTLE with momentum reversal and momentum reversal) preserves the measure  $\mu$ . By combining these three steps as in Algorithm 2, we obtain a Markov chain which does not only leave  $\mu$  invariant but is actually reversible up to momentum reversal with respect to  $\mu$ . Notice that combining the last Step 10 and the first Step 3 of Algorithm 2 is actually equivalent to performing a single momentum update with a parameter  $\alpha^2$ .*

As in Theorem 1, one still needs to verify irreducibility in order to prove the ergodicity of the Markov chain generated by Algorithm 2. We also refer here to [7, 9, 26, 33] for related results in the unconstrained case and to [15] for results involving constraints.

Before concluding this section, let us compare Algorithms 1 and 2. As already mentioned, when  $M = I_d$  and momenta are fully resampled, *i.e.*  $\alpha = 0$  in (39), Algorithm 2 is exactly the same as Algorithm 1, when considering only the position variable on  $\Sigma$ . When  $\alpha \neq 0$ , however, the chain in the position variable obtained from Algorithm 2 is not Markovian since momenta are only partially refreshed. This may be useful to prevent the system going back towards the

previous position. Let us mention incidentally that it would be interesting to derive quantitative results supporting this reasoning.

Concerning the proofs of reversibility (see Section 4), the draw of the velocity and the update of position are considered as a whole in our analysis of Algorithm 1, following [37]. Algorithm 2 is analyzed differently, as the composition of separate steps which leave the measure  $\mu$  invariant, namely the resampling of momentum, the momentum reversal and finally the metropolization of the update by the deterministic (set-valued) map  $\Phi$ , in the spirit of [24]. These two approaches give different insights on the reversibility properties of these algorithms.

### 2.3 Numerical computation of the constraint equations

In this short section, we explain how set-valued proposal maps can be obtained numerically for different types of maps  $\xi : \mathbb{R}^d \rightarrow \mathbb{R}^k$ , and then we discuss how Assumptions 2 and 3 are satisfied in practice. We distinguish two situations, depending on whether all solutions of the constraint equations (10) and (27b) are guaranteed to be found or not. It is obvious that the numerical solvers discussed below find (at most) a finite number of solutions, so that the first item of Assumption 2 (resp. Assumption 3) is satisfied in practice.

**Case 1: All solutions of the constraint equation are guaranteed to be found.** In some specific situations, all the solutions to the equations (10) and (27b) can be analytically computed. More generally, when  $\xi$  is a scalar valued polynomial, all the solutions are guaranteed to be found up to an arbitrary small numerical precision. Indeed, in this case, numerical algorithms can be used to compute all the roots of a univariate polynomial, such as the Julia package `PolynomialRoots.jl` [34].

Let us discuss in this case the assumptions in the second item of Assumptions 2 and 3. The analysis in Section 2.1.1 (see in particular Proposition 1) implies that if one defines  $\Psi_x(v) = \mathcal{F}_x(v) \setminus C_x$  (where  $C_x$  is defined by (6)), then  $\mathcal{D} = \{(x, y) \in \Sigma \times \Sigma \mid \det(\nabla \xi(y)^T \nabla \xi(x)) \neq 0\}$ . Similarly, for HMC, the function  $\Phi$  can be defined as  $\Phi(z) = \mathcal{F}(z) \setminus C_{M, \Pi(z)}$  (where the set  $C_{M, x}$  is defined by (33) and  $\Pi$  is defined by (37)), and then, the set  $\mathcal{D}_\Phi$  in Assumption 3 is:

$$\mathcal{D}_\Phi = \left\{ (z, z') \in T^*\Sigma \times T^*\Sigma \mid \exists x, x' \in \Sigma \times \Sigma, \det(\nabla \xi(x')^T M^{-1} \nabla \xi(x)) \neq 0, \right. \\ \left. z = (x, G_{M, x}(x')), z' = (x', G_{M, x'}(x)) \right\},$$

where  $G_{M, x}$  is the map defined in (31). From the above definition, both sets  $\mathcal{D}$  and  $\mathcal{D}_\Phi$  are non-empty for any timestep  $\tau > 0$ . The regularity properties in the third items of Assumptions 2 and 3 are then given by Propositions 1 and 3.

**Case 2: All solutions of the constraint equation cannot be guaranteed to be found.** When  $\xi$  is either a multidimensional polynomial, or a nonlinear function, there are in general no numerical methods for computing all solutions of the constraint equations. The numerical methods under consideration can sometimes find all solutions, but sometimes only a subset of them.

When the map  $\xi : \mathbb{R}^d \rightarrow \mathbb{R}^k$  is defined by polynomials, the constraint equations (10) and (27b) are polynomial systems. Finding numerical solutions of polynomial systems is in fact a well

studied topic in the field of numerical algebraic geometry [35], where the primary computational approach is the homotopy continuation method. In particular, there are theoretical results in algebraic geometry (*e.g.*, Bertini’s theorem [17]) which guarantee that the homotopy continuation method is able to compute all solutions of polynomial systems in principle – although the actual computation of all solutions may not be achieved in practice due to various numerical and implementation issues. The homotopy continuation method has been implemented in several numerical packages, such as Bertini [3] and HomotopyContinuation.jl [5]. They can be used to solve multiple solutions of polynomial systems.

For generic nonlinear constraints, Newton’s method is commonly used to solve the constraint equations, as done in [21, 23, 37, 24]. It finds a solution provided that the initial guess is not too far away from some solution. In general, it has a fast (local) convergence rate and is easy to implement. Multiple solutions of the constraint equations can be computed by applying Newton’s method with different initial guesses.

Let us finally discuss the second item of Assumptions 2 and 3 for the set-valued proposal maps obtained by the methods discussed here. It is expected that the set  $\mathcal{D}$  in Assumption 2 (resp. the set  $\mathcal{D}_\Phi$  in Assumption 3) will be non-empty provided that the timestep  $\tau$  is not too large, in particular when Newton’s method is used (see [24, Lemma 2.8] for a related result).

The regularity properties in the third items of Assumptions 2 and 3 need to be checked for the specific numerical method at hand; see [24, Section 2.3.3] for the Newton scheme. More precisely, for Assumption 2, Proposition 1 implies that one can choose  $\mathcal{O} = \cap_{j=1}^m G_x(\mathcal{Q}_j)$ , where  $m = |\Psi_x(v) \setminus C_x|$ , and define  $\Psi_x^{(j)}(\bar{v}) = (G_x|_{\mathcal{Q}_j})^{-1}(\bar{v})$  for  $\bar{v} \in \mathcal{O}$ , where  $\mathcal{Q}_j$  is the neighborhood of  $y_j$  such that  $G_x|_{\mathcal{Q}_j}$  is a  $C^1$ -diffeomorphism. Therefore, the third item of Assumption 2 will be satisfied as long as the solutions  $\Psi_x^{(j)}(\bar{v})$  can be numerically computed for  $\bar{v}$  belonging to a neighborhood of  $v$ . For a numerically computed point  $y_j \in \Psi_x(v)$  such that the non-tangential condition in [24, Definition 2.1] is satisfied (*i.e.*  $y_j \in \Psi_x(v) \setminus C_x$ ), the numerical solvers typically behave continuously for  $\bar{v}$  belonging to a neighborhood of  $v$  (see [24, Section 2.3.3] for a discussion concerning Newton’s method), and thus, it is expected that  $\Psi_x^{(j)}(\bar{v})$  is indeed in the list of the numerical solutions for  $\bar{v}$  belonging to a neighborhood of  $v$ . Likewise, for Assumption 3, since  $\Pi(z_j) \notin C_{M, \Pi(z)}$  for  $1 \leq j \leq m$ , Proposition 3 implies that one can choose  $\Phi^{(j)}(\bar{z}) = \Upsilon^{(j)}(\bar{z})$  for  $\bar{z} \in \mathcal{O} = \cap_{j=1}^m \mathcal{O}_j$ , where  $\mathcal{O}_j$  is the neighborhood of  $z$  and  $\Upsilon^{(j)} : \mathcal{O}_j \rightarrow \Upsilon^{(j)}(\mathcal{O}_j) \subset T^*\Sigma$  is the  $C^1$ -diffeomorphism considered in the third item of Proposition 3 for  $z' = z_j$ . Therefore, the third item of Assumption 3 is satisfied as long as the solutions  $\Phi^{(j)}(\bar{z})$  can be numerically computed for  $\bar{z}$  belonging to a neighborhood of  $z$ , which is again expected to be the case for many numerical solvers.

### 3 Numerical examples

We illustrate the algorithms introduced in Section 2 to sample probabilities measures on two submanifolds: a two-dimensional torus in a three-dimensional space (see Section 3.1), already considered in [37, 24]; and disconnected components which are subsets of a nine-dimensional sphere (see Section 3.2). We use Algorithm 2 with  $M = I_d$  and varying  $\tau$  and  $\alpha$ . Remember that when  $\alpha = 0$ , since the mass is the identity, Algorithm 2 is equivalent to Algorithm 1. All simulations were done using the Julia programming language (see <https://github.com/zwpku/Constrained-HMC>)

for the codes) and carried out on the same desktop computer which has 8 CPUs (Intel Xeon E3-1245), 8G memory, and operating system Debian 10.

### 3.1 Two-dimensional torus in a three-dimensional space

In this example, we apply Algorithm 2 to study a two-dimensional torus in  $\mathbb{R}^3$  (see Figure 2, left). More precisely, the torus is a two-dimensional submanifold of  $\mathbb{R}^3$  defined as the solution in  $(x_1, x_2, x_3)$  of the equation

$$\left(R - \sqrt{x_1^2 + x_2^2}\right)^2 + x_3^2 - r^2 = 0, \quad x = (x_1, x_2, x_3)^T \in \mathbb{R}^3, \quad (42)$$

where  $0 < r < R$ . After simple algebraic calculations, we see that (42) is equivalent to the polynomial equation

$$\xi(x) = 0, \quad \text{where } \xi(x) = (R^2 - r^2 + x_1^2 + x_2^2 + x_3^2)^2 - 4R^2(x_1^2 + x_2^2). \quad (43)$$

Therefore, the torus is the zero level set  $\Sigma$  of the polynomial  $\xi$  as defined in (43). In the following, we will use the following parametrization of the torus:

$$x_1 = (R + r \cos \phi) \cos \theta, \quad x_2 = (R + r \cos \phi) \sin \theta, \quad x_3 = r \sin \phi, \quad (44)$$

where  $(\phi, \theta) \in [0, 2\pi)^2$ . In particular, it can be verified that the normalized surface measure of the torus in the variables  $\theta, \phi$  (still denoted by  $\sigma_\Sigma$  with some abuse of notation) is given by

$$\sigma_\Sigma(d\phi d\theta) = \frac{1}{2\pi} \left(1 + \frac{r}{R} \cos \phi\right) d\phi d\theta. \quad (45)$$

To apply Algorithm 2, the constraint equation (27b) needs to be solved to compute the set  $\Phi(x, p)$ . Since  $\xi$  defined by (43) is a fourth order polynomial, (27b) has at most four real solutions. In this experiment, besides Newton’s method that provides at most one solution of (27b) for a given initial guess, we also apply the Julia packages PolynomialRoots.jl [34] and HomotopyContinuation.jl [5], which can compute multiple solutions of (27b). Since each iteration of Algorithm 2 preserves the target distribution regardless of the choice of the numerical solver, we can also use different solvers to compute  $\Phi(x, p)$  in different MCMC iterations. By exploiting the freedom provided by Algorithm 2, we obtain the following schemes that we will use in the subsequent numerical tests (see also the summary in Table 1):

- “Newton”, where Newton’s method is used to compute the set  $\Phi(x, p)$  at each MCMC iteration.
- “PR” (“Hom”), where the PolynomialRoots.jl (resp. the HomotopyContinuation.jl) Julia package is used at each MCMC iteration to compute the set  $\Phi(x, p)$  and one state is chosen randomly with uniform probability.
- “PR-far” (“Hom-far”), where the PolynomialRoots.jl (resp. the HomotopyContinuation.jl) Julia package is used at each MCMC iteration to compute the set  $\Phi(x, p)$ . The states in  $\Phi(x, p)$  are sorted in ascending order based on the Euclidean distances between their

position components and the current position  $x$ , and one state is randomly chosen according to the probability distributions in Table 2.

- Scheme “PR50-far” (“Hom50-far”), where the set  $\Phi(x, p)$  is computed using PolynomialRoots.jl (HomotopyContinuation.jl) Julia package every 50 MCMC iterations, while Newton’s method is used in the other iterations. As in the previous item, when multiple states in  $\Phi(x, p)$  are obtained, they are sorted in ascending order based on the Euclidean distances between their position components to the current position  $x$ , and one state is chosen randomly according to the probability distributions in Table 2.

Note that in the schemes “\*-far”, the probability distributions in Table 2 slightly favors states that are at larger distances from the current state. As hybrid schemes, we expect “PR50-far” and “Hom50-far” to have a better sampling efficiency to explore the space than ”Newton”, together with a lower computational cost than “PR” (“Hom”) or “PR-far” (“Hom-far”).

Scheme	Solver	Period	Distribution $\omega(\cdot   \cdot)$
Newton	Newton	N/A	N/A
PR	PolynomialRoots	1	uniform
PR-far	PolynomialRoots	1	non-uniform
PR50-far	Newton + PolynomialRoots	50	non-uniform
Hom	HomotopyContinuation	1	uniform
Hom-far	HomotopyContinuation	1	non-uniform
Hom50-far	Newton + HomotopyContinuation	50	non-uniform

Table 1: Sampling schemes on the torus based on Algorithm 2. For each scheme, the column “Solver” shows the numerical solvers used for solving the constraint equation (27b). The column “Period” shows how often multiple solutions of the constraint equation are computed, using either the PolynomialRoots.jl or HomotopyContinuation.jl Julia packages. When multiple solutions (states) are found, one state is chosen randomly according to either a uniform distribution (“uniform”) or to the probability distributions in Table 2 (“non-uniform”).

We fix  $R = 1.0$  and  $r = 0.5$  in (42)–(45). In each test, we run  $N = 10^7$  MCMC iterations using Algorithm 2, with either  $\alpha = 0$  or  $\alpha = 0.7$  in (39) for updating the momenta  $p$ . When Newton’s method is used to compute  $\Phi(x, p)$ , the Lagrange multiplier is set to zero initially and the convergence criterion is based on the Euclidean norm of  $\xi$  being sufficiently small, namely  $|\xi(x)| < 10^{-8}$ . At most 10 Newton’s iterations are performed to solve the constraint equation. As explained above, when multiple proposal states are found (by the PolynomialRoots.jl or HomotopyContinuation.jl Julia packages), we randomly choose one state either with uniform probability or according to the probability distributions shown in Table 2, based on the Euclidean distances of their position components to the current position  $x$ . In the reversibility check step of Algorithm 2, two states are considered the same if their Euclidean distance in position component is less than  $10^{-6}$ .

**Remark 6.** *Let us mention that it is important to choose the tolerance for the reversibility check larger than the tolerance for the convergence of the Newton algorithm. When the tolerance for the reversibility check is too small, it may happen that the two states are in fact the same, but, due to the incomplete convergence of the Newton step and/or numerical round-off errors, the states are considered to be different.*

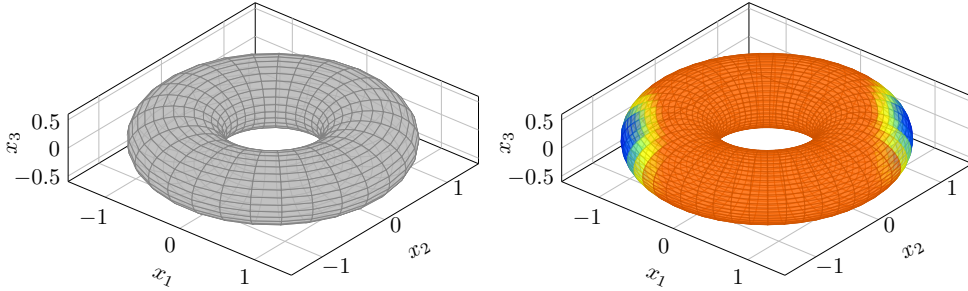


Figure 2: Left: Torus in  $\mathbb{R}^3$ . Right: Potential  $V(x)$  in (46) on the torus (blue color corresponds to low values of potential). The function  $V$  has two local minima at  $((R+r)/\sqrt{2}, (R+r)/\sqrt{2}, 0)$  and  $(-(R+r)/\sqrt{2}, -(R+r)/\sqrt{2}, 0)$ .

$n$	$\omega(z_1   z)$	$\omega(z_2   z)$	$\omega(z_3   z)$	$\omega(z_4   z)$
1	1.0			
2	0.4	0.6		
3	0.2	0.4	0.4	
4	0.2	0.3	0.3	0.2

Table 2: Non-uniform probability distributions  $\omega$ . At each  $z = (x, p)$ , assuming that  $\Phi(z) = \{z_1, \dots, z_n\}$ ,  $1 \leq n \leq 4$ , where the states  $z_j$  are sorted in ascending order according to the distances of their position components to the current position  $x$ , one state  $z_j$  is chosen randomly according to the probability distribution  $\omega(\cdot | z)$  on the corresponding row.

**Uniform law on the torus.** We start by considering the sampling of the distribution  $\sigma_\Sigma$  in (45), *i.e.*  $V = 0$ . The aim is to validate Algorithm 2 and to investigate the performance of the different sampling schemes in Table 1. In each case, we choose the step-size  $\tau = 0.8$  in the one-step RATTLE with momentum reversal scheme (29). The results are summarized in Tables 3–4 and Figure 3. We see from Figure 3 that all schemes in Table 1 are able to correctly sample the distribution (45) of the angles  $\phi, \theta$  with  $N = 10^7$  samples (results with  $\alpha = 0.7$  are very similar and therefore are not shown). As expected, Table 3 confirms that sampling schemes using either `PolynomialRoots.jl` or `HomotopyContinuation.jl` Julia packages can find multiple solutions of the constraint equation. Note that the empirical probability to find more than one states is smaller for “PR50-far” and “Hom50-far” simply because multiple solutions are sought only every 50 MCMC iterations. In Table 4, we show the average jump distance when the system jumps to a new state, *i.e.*, the average value of  $|x^{(i+1)} - x^{(i)}|$  among the MCMC iterations such that  $x^{(i+1)} \neq x^{(i)}$ . As shown in the column “Distance” in Table 4, using multiple proposal states in  $\Phi(x, p)$  leads to larger jump distances on average for the Markov chains. At the same time, we observe that the `PolynomialRoots.jl` package is slightly faster than the `HomotopyContinuation.jl` Julia package, but both packages are computationally more expensive than Newton’s method. The two (hybrid) schemes “PR50-far” and “Hom50-far”, which use the `PolynomialRoots.jl` and `HomotopyContinuation.jl` packages every 50 iterations, require run-times ( $1.8 \times 10^3$  seconds) similar to the ones for “Newton” ( $1.6 \times 10^3$  seconds), but at the same time also allow the Markov chains to make large (non-local) jumps when multiple solutions are computed. From Table 3 and Table 4 we can also observe that the results computed using both  $\alpha = 0$  and  $\alpha = 0.7$  are very similar for this example (In fact, the results are similar for a very wide range of values

of  $\alpha$ ).

$\alpha$	Scheme	No. of solutions in forward step				No. of solutions in reversibility check			
		0	1	2	4	0	1	2	4
0.0	Newton	48.0%	52.0%	0.0%	0.0%	1.2%	98.8%	0.0%	0.0%
	PR	45.9%	0.0%	49.9%	4.2%	0.0%	0.0%	91.2%	8.8%
	PR-far	45.9%	0.0%	49.9%	4.2%	0.0%	0.0%	91.3%	8.7%
	PR50-far	48.0%	50.9%	1.0%	0.1%	1.2%	96.8%	1.9%	0.2%
	Hom	46.0%	0.0%	49.9%	4.1%	0.0%	0.0%	91.2%	8.8%
	Hom-far	45.9%	0.0%	49.9%	4.2%	0.0%	0.0%	91.3%	8.6%
	Hom50-far	48.0%	50.9%	1.0%	0.1%	1.2%	96.8%	1.9%	0.2%
0.7	Newton	48.0%	52.0%	0.0%	0.0%	1.2%	98.8%	0.0%	0.0%
	PR	45.9%	0.0%	49.9%	4.1%	0.0%	0.0%	91.2%	8.8%
	PR-far	45.9%	0.0%	49.9%	4.2%	0.0%	0.0%	91.3%	8.7%
	PR50-far	48.0%	50.9%	1.0%	0.1%	1.1%	96.8%	1.9%	0.2%
	Hom	45.9%	0.0%	49.9%	4.1%	0.0%	0.0%	91.2%	8.8%
	Hom-far	45.9%	0.0%	49.9%	4.2%	0.0%	0.0%	91.3%	8.7%
	Hom50-far	48.0%	50.9%	1.0%	0.1%	1.2%	96.8%	1.9%	0.2%

Table 3: Sampling of the uniform law on the torus. The percentages in “forward step” are the proportions of MCMC iterations among the total number  $N = 10^7$  of MCMC iterations where  $i$  state(s) are found in the set  $\Phi(x, p)$ . The percentages in “reversibility check” are the proportions of the number of MCMC iterations where  $i$  state(s) are found in the set  $\Phi(x^1, p^{1,-})$  (where  $(x^1, p^{1,-}) \in \Phi(x, p)$  is the selected proposal state) for MCMC iterations where the reversibility check step has been invoked (*i.e.* when at least one state has been found in  $\Phi(x, p)$  in the forward step).

**Bimodal distribution on the torus.** In the second task, we apply Algorithm 2 to sample a bimodal distribution on the torus. The aim is to demonstrate that using multiple proposal states in  $\Phi(x, p)$  can improve the sampling efficiency of MCMC schemes by introducing non-local jumps in Markov chains. We consider the target distribution (2) with  $\beta = 20$  and (see Figure 2, right)

$$V(x) = (x_1 - x_2)^2 + 5 \left( \frac{x_1^2 + x_2^2}{(R+r)^2} - 1 \right)^2. \quad (46)$$

The potential has two global minima on  $\Sigma$  at  $\left( \frac{R+r}{\sqrt{2}}, \frac{R+r}{\sqrt{2}}, 0 \right)$  and  $\left( -\frac{R+r}{\sqrt{2}}, -\frac{R+r}{\sqrt{2}}, 0 \right)$ .

We simulate the distributions of the two angles  $\phi, \theta$  in (44) using the schemes “Newton”, “PR”, “PR50-far”, “Hom”, and “Hom50-far” from Table 1 with both  $\alpha = 0$  and  $\alpha = 0.7$  (the two schemes “PR-far” and “Hom-far” are not used because they provide results similar to those of “PR” and “Hom”, respectively). The step-size in the one-step RATTLE with momentum reversal scheme (29) is set to  $\tau = 0.8$ . The value of the timestep is chosen in order to offer some empirical optimal trade-off in terms of sampling the equilibrium measure at hand. The values of the other parameters are the same as in the first sampling task. The numerical results are summarized in Tables 5–6 and Figures 4–5. From Figure 4, we observe that, unlike the schemes “PR”, “PR50-far”, “Hom” and “Hom50-far”, the scheme “Newton” still could not reproduce the correct density profile of  $\theta$  within  $N = 10^7$  sampled states. Figure 5 shows that, in the scheme “Newton”, the transition of the Markov chain from the basin of one local minimum to the basin



$\alpha$	Scheme	FSR	BSR	TAR	Distance	Time (s)
0.0	Newton	0.52	0.90	0.45	0.73	$1.6 \times 10^3$
	PR	0.54	1.00	0.44	1.13	$5.7 \times 10^3$
	PR-far	0.54	1.00	0.43	1.18	$5.9 \times 10^3$
	PR50-far	0.52	0.90	0.45 (0.43)	0.74 (1.18)	$1.6 \times 10^3$
	Hom	0.54	1.00	0.44	1.13	$8.4 \times 10^3$
	Hom-far	0.54	1.00	0.43	1.18	$8.9 \times 10^3$
	Hom50-far	0.52	0.90	0.45 (0.43)	0.74 (1.18)	$1.8 \times 10^3$
0.7	Newton	0.52	0.90	0.45	0.73	$1.6 \times 10^3$
	PR	0.54	1.00	0.44	1.13	$5.8 \times 10^3$
	PR-far	0.54	1.00	0.43	1.18	$5.4 \times 10^3$
	PR50-far	0.52	0.90	0.45 (0.43)	0.74 (1.18)	$1.8 \times 10^3$
	Hom	0.54	1.00	0.44	1.13	$8.9 \times 10^3$
	Hom-far	0.54	1.00	0.43	1.18	$8.3 \times 10^3$
	Hom50-far	0.52	0.90	0.45 (0.43)	0.74 (1.18)	$1.8 \times 10^3$

Table 4: Sampling of the uniform law on the torus. The column “FSR” (short for “forward success rate”) shows the ratios of MCMC iterations within  $N = 10^7$  MCMC iterations where at least one state is found in  $\Phi(x, p)$  as a proposal state. The column “BSR” (short for “backward success rate”) shows the ratios of the number of MCMC iterations for which the reversibility check step is successful, within the total number of MCMC iterations where the reversibility check step is invoked. The column “TAR” (short for “total acceptance rate”) displays the proportions of MCMC iterations within  $N = 10^7$  iterations in which the system jumps to a new state. The column “Distance” shows the average jump distance of the position component, provided that the system jumps to a new position. For each scheme, the run-time (seconds) spent in performing  $N = 10^7$  MCMC iterations is shown in the column “Time (s)”. For the (hybrid) schemes “PR50-far” and “Hom50-far”, the average jump rates and the average jump distances among the MCMC iterations for which the set  $\Phi(x, p)$  is computed using either the PolynomialRoots.jl or HomotopyContinuation.jl packages (*i.e.* every 50 iterations; in total  $2 \times 10^5$  times) are shown in bracket.

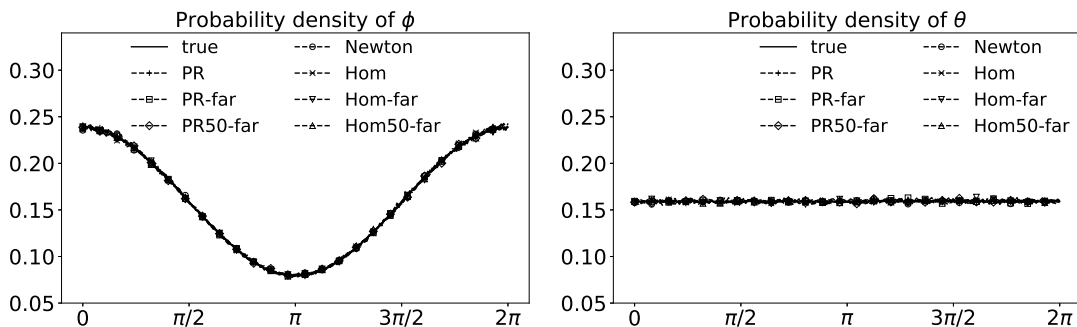


Figure 3: Sampling of the uniform law on the torus (for  $\alpha = 0$ ). Probability density profiles of the two angles  $\phi, \theta$  in (44), estimated from  $N = 10^7$  sampled states using different schemes in Table 1 with  $\alpha = 0$ . The curves with label “true” are the reference probability density functions computed from (45).

of the other one rarely happens, due to the bimodality of the target distribution, implying that a larger sample size is needed in order to correctly sample the target distribution using the “Newton” scheme. On the other hand, by computing multiple proposal states in  $\Phi(x, p)$ , the Markov chains in the schemes “PR”, “PR50-far”, “Hom” and “Hom50-far” are able to perform non-local jumps, as shown in Tables 5–6. To investigate the effect of these non-local jumps, in the column “Large jump rate” of Table 6 we record the frequency of MCMC iterations when the first component  $x_1$  of the state  $x$  changes its sign among the total  $N = 10^7$  iterations. This can be used as an indicator for the occurrence of large jumps from one local minimum to the other. We see that the frequencies of large jumps are higher when multiple proposal states are computed, leading to better sampling performances compared to the scheme “Newton”. In particular, the two hybrid schemes “PR50-far” and “Hom50-far” achieve better sampling efficiency with computational cost ( $2.0 \times 10^3$  seconds) similar to the one for the scheme “Newton” ( $1.7 \times 10^3$  seconds). Finally, from Table 5 and Table 6, we can again observe that the results computed using both  $\alpha = 0$  and  $\alpha = 0.7$  are very similar for this test example (As in the previous test example, the results are in fact similar for a very wide range of values of  $\alpha$ ).

$\alpha$	Scheme	No. of solutions in forward step				No. of solutions in reversibility check			
		0	1	2	4	0	1	2	4
0.0	Newton	2.2%	97.8%	0.0%	0.0%	0.0%	100.0%	0.0%	0.0%
	PR	2.1%	0.0%	51.8%	46.1%	0.0%	0.0%	75.2%	24.8%
	PR50-far	2.2%	95.8%	1.0%	0.9%	0.0%	98.0%	1.6%	0.5%
	Hom	2.1%	0.0%	51.8%	46.1%	0.0%	0.0%	75.2%	24.8%
	Hom50-far	2.2%	95.8%	1.0%	0.9%	0.0%	98.0%	1.6%	0.5%
0.7	Newton	2.2%	97.8%	0.0%	0.0%	0.0%	100.0%	0.0%	0.0%
	PR	2.1%	0.0%	51.8%	46.0%	0.0%	0.0%	75.2%	24.8%
	PR50-far	2.2%	95.8%	1.0%	0.9%	0.0%	98.0%	1.6%	0.5%
	Hom	2.1%	0.0%	51.8%	46.1%	0.0%	0.0%	75.2%	24.8%
	Hom50-far	2.2%	95.8%	1.0%	0.9%	0.0%	98.0%	1.5%	0.5%

Table 5: Sampling of the bimodal distribution on the torus. See Table 3 for the meanings of the percentages. The schemes “PR-far” and “Hom-far” in Table 1 provide similar results, which are not reported here.

$\alpha$	Scheme	FSR	BSR	TAR	Large jump rate	Time (s)
0.0	Newton	0.98	1.00	0.60	$2.0 \times 10^{-7}$	$1.7 \times 10^3$
	PR	0.98	1.00	0.22	$4.0 \times 10^{-3}$	$7.5 \times 10^3$
	PR50-far	0.98	1.00	0.60 (0.17)	$6.5 \times 10^{-5}$	$1.8 \times 10^3$
	Hom	0.98	1.00	0.22	$4.0 \times 10^{-3}$	$1.2 \times 10^4$
	Hom50-far	0.98	1.00	0.60 (0.18)	$6.7 \times 10^{-5}$	$2.0 \times 10^3$
0.7	Newton	0.98	1.00	0.60	0.0	$1.7 \times 10^3$
	PR	0.98	1.00	0.22	$4.0 \times 10^{-3}$	$6.9 \times 10^3$
	PR50-far	0.98	1.00	0.60 (0.17)	$6.5 \times 10^{-5}$	$1.9 \times 10^3$
	Hom	0.98	1.00	0.22	$4.0 \times 10^{-3}$	$9.9 \times 10^3$
	Hom50-far	0.98	1.00	0.60 (0.18)	$6.3 \times 10^{-5}$	$1.9 \times 10^3$

Table 6: Sampling of the bimodal distribution on the torus. See Table 4 for the meaning of each column. The column “Large jump rate” records the frequency of MCMC iterations when the first component  $x_1$  of the state  $x$  changes its sign among the total  $N = 10^7$  iterations.

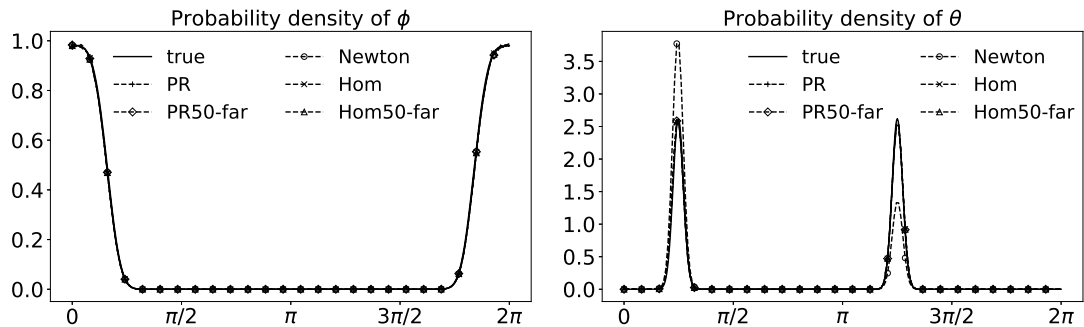


Figure 4: Sampling of the bimodal distribution on the torus (for  $\alpha = 0$ ). Probability density profiles of the two angles  $\phi, \theta$  in (44), estimated from  $N = 10^7$  sampled states using different schemes from Table 1 with  $\alpha = 0$ . (The results for both the schemes “PR-far” and “Hom-far”, as well as for  $\alpha = 0.7$ , are similar and therefore not reported.) The plots with label “true” are the reference probability density functions computed from (45) and (46).

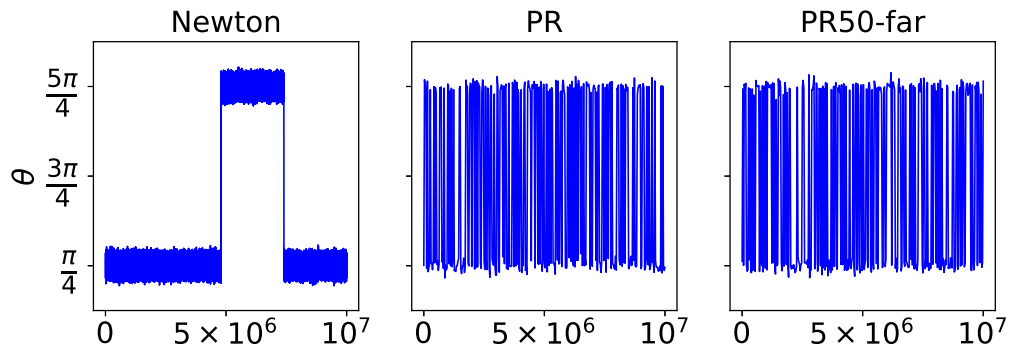


Figure 5: Sampling of the bimodal distribution on the torus (for  $\alpha = 0$ ). Sample trajectories of the angle  $\theta$  in (44) for the schemes “Newton”, “PR”, and “PR50-far” (see Table 1) with  $\alpha = 0$ . To have a good visual effect, sampled states are plotted every 10 iterations in “Newton”, while in both “PR” and “PR50-far” sampled states are shown every 3000 iterations. The results should be analyzed together with the column “Large jump rate” in Table 6. Trajectories for the schemes “Hom” and “Hom50-far” are not reported here because they are very similar to those of “PR” and “PR50-far”, respectively.

### 3.2 Disconnected components on a nine-dimensional sphere

In the second example, we consider the level set  $\Sigma = \{x \in \mathbb{R}^{10} \mid \xi(x) = 0 \in \mathbb{R}^2\}$ , where  $\xi : \mathbb{R}^{10} \rightarrow \mathbb{R}^2$  is given by

$$\xi_1(x) = \frac{1}{2} \left( \sum_{i=1}^{10} x_i^2 - 9 \right), \quad \xi_2(x) = x_1 x_2 x_3 - 2, \quad (47)$$

for  $x = (x_1, x_2, \dots, x_{10}) \in \mathbb{R}^{10}$ . Note that  $\Sigma$  is a 8-dimensional submanifold in  $\mathbb{R}^{10}$  composed of 4 connected components due to the second constraint  $\xi_2(x) = x_1 x_2 x_3 - 2 = 0$ . Let us denote these 4 connected components by

$$\begin{aligned} \mathcal{C}_0 &= \{x \in \Sigma \mid x_1 > 0, x_2 > 0, x_3 > 0\}, \\ \mathcal{C}_1 &= \{x \in \Sigma \mid x_1 > 0, x_2 < 0, x_3 < 0\}, \\ \mathcal{C}_2 &= \{x \in \Sigma \mid x_1 < 0, x_2 > 0, x_3 < 0\}, \\ \mathcal{C}_3 &= \{x \in \Sigma \mid x_1 < 0, x_2 < 0, x_3 > 0\}. \end{aligned} \quad (48)$$

We apply Algorithm 2 with  $\alpha = 0$  to sample the probability measure (2) with  $\beta = 1.0$  and  $V(x) = \frac{1}{2}(x_1 - 0.6)^2$ . The following three schemes are used in the following numerical experiments:

- “Newton”, where Newton’s method is used to compute the set  $\Phi(x, p)$  at each MCMC iteration.
- “Hom”, where the HomotopyContinuation.jl Julia package is used at each iteration to compute the set  $\Phi(x, p)$ , and one state is randomly chosen with uniform probability.
- “Hom10”, where the set  $\Phi(x, p)$  is computed using the HomotopyContinuation.jl Julia package every 10 MCMC iterations, while Newton’s method is used for the other iterations. As in the previous item, when multiple states in  $\Phi(x, p)$  are obtained, one state is randomly chosen with uniform probability.

In contrast to the example of Section 3.1, the PolynomialRoots.jl Julia package cannot be used since  $\xi$  is vector-valued. Also, the scheme “Hom10” is used instead of “Hom50” (in the previous example), because we observe that it is important to compute multiple solutions more frequently in order to sample the various components of  $\Sigma$ . In each simulation,  $N = 10^7$  MCMC iterations are performed using Algorithm 2, with step-size  $\tau = 0.5$ .

As shown in Table 7, multiple proposal states are found in the MCMC iterations for both the “Hom” and “Hom10” schemes. The empirical density distributions of the state’s components  $x_1$ ,  $x_2$ , and  $x_4$  under the target distribution  $\nu$  are shown in Figure 6. (Due to the symmetry of  $\Sigma$  and the choice of potential  $V$ ,  $x_3$  has the same distribution as  $x_2$ , while  $x_5, x_6, \dots, x_{10}$  have the same distribution as  $x_4$ .) While the same distributions of  $x_1$  and  $x_4$  are obtained using all three schemes, we observe that the distribution of  $x_2$  provided by the “Newton” scheme is different from the results given by the schemes “Hom” and “Hom10”. The distribution of  $x_2$  with “Newton” is clearly far from the ground truth since it is not even.

To have a better understanding of the performance of the different schemes, let us investigate the sampling of the four connected components  $\mathcal{C}_0, \mathcal{C}_1, \mathcal{C}_2, \mathcal{C}_3$  in each scheme. First of all, it is

easy to see that  $\mathcal{C}_0$  and  $\mathcal{C}_1$  have the same probability under  $\nu$ , while  $\mathcal{C}_2$  and  $\mathcal{C}_3$  also have the same (smaller than  $\mathcal{C}_0$  and  $\mathcal{C}_1$ ) probability under  $\nu$ . With this observation, from the last four columns of Table 8, we can already conclude that while both the “Hom” and “Hom10” schemes provide reasonable probabilities, the probabilities estimated using the “Newton” scheme are inaccurate. This indicates that the sample size  $N = 10^7$  is still not enough for the “Newton” scheme to correctly estimate the probability of each connected component. In Figure 7, the transitions among the components  $\mathcal{C}_i$  for  $0 \leq i \leq 3$  are shown for the three different schemes. We see that, in the “Newton” scheme, the state of the Markov chain stays within the same connected component most of the time and the change from one component to another happens very rarely (in total 18 times in  $10^7$  iterations). This implies that Newton’s method mostly proposes moves to states within a connected component, which is indeed expected. On the other hand, from Figure 7 we observe that the transitions among the connected components occur frequently both for “Hom” and “Hom10”. To provide more details, we plot in Figure 8 the transitions among the connected components as directed graphs, whose nodes and edges represent the four components  $\mathcal{C}_i$  and the transitions among the components, respectively. The frequency of the transition from one connected component  $\mathcal{C}_i$  to another component  $\mathcal{C}_j$  for  $0 \leq i \neq j \leq 3$ , is shown on the edge from node  $i$  to node  $j$ . The total frequency of transitions in each scheme is also given in the column “CTF” of Table 8. These results show that finding multiple proposal states in Algorithm 2 is helpful, particularly when the submanifold  $\Sigma$  contains multiple connected components. Finally, let us emphasize that the hybrid scheme “Hom10” achieves a much better sampling efficiency than the “Newton” scheme for a comparable computational cost (Table 8).

Scheme	No. of solutions in forward step					No. of solutions in reversibility check				
	0	1	2	4	6	0	1	2	4	6
Newton	15.9%	84.1%	0.0%	0.0%	0.0%	0.1%	99.9%	0.0%	0.0%	0.0%
Hom	13.3%	0.0%	76.6%	9.8%	0.2%	0.0%	0.0%	84.7%	15.2%	0.1%
Hom10	15.7%	75.7%	7.7%	1.0%	0.0%	0.1%	89.6%	8.7%	1.6%	0.0%

Table 7: Sampling of the 9D sphere. See Table 3 for the meaning of the percentages. It is possible to find 3 or 5 states in “Hom” and “Hom10”, but their percentages are below 0.1%.

Scheme	FSR	BSR	Jump rate	CTF	Time (s)	Prob. in each component			
						$\mathcal{C}_0$	$\mathcal{C}_1$	$\mathcal{C}_2$	$\mathcal{C}_3$
Newton	0.84	1.00	0.76	$1.8 \times 10^{-6}$	$2.4 \times 10^3$	0.44	0.37	0.15	0.03
Hom	0.87	1.00	0.43	$9.4 \times 10^{-3}$	$2.5 \times 10^4$	0.40	0.39	0.11	0.10
Hom10	0.84	1.00	0.73	$9.3 \times 10^{-4}$	$4.8 \times 10^3$	0.39	0.39	0.10	0.11

Table 8: Sampling of the 9D sphere. The column “CTF” (short for “component transition frequency”) shows the frequency at which the Markov chain jumps from one component to another in  $N = 10^7$  MCMC iterations. The empirical probabilities of visits to a component along a trajectory are shown in the last four columns. See Table 4 for the meaning of the other columns (*i.e.*, “FSR”, “BSR”, “Jump rate”, and “Time (s)”).

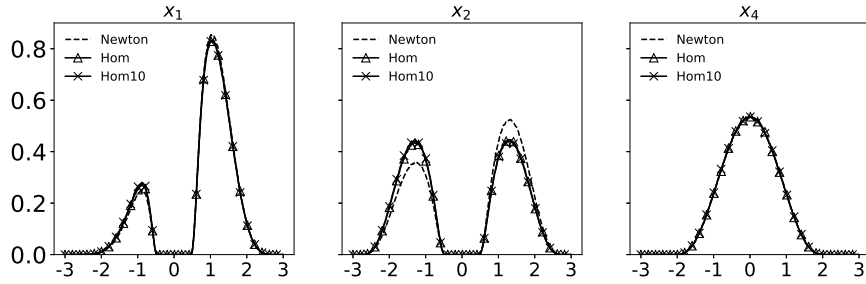


Figure 6: Sampling of the 9D sphere: empirical probability densities of  $x_1$ ,  $x_2$  and  $x_4$ .

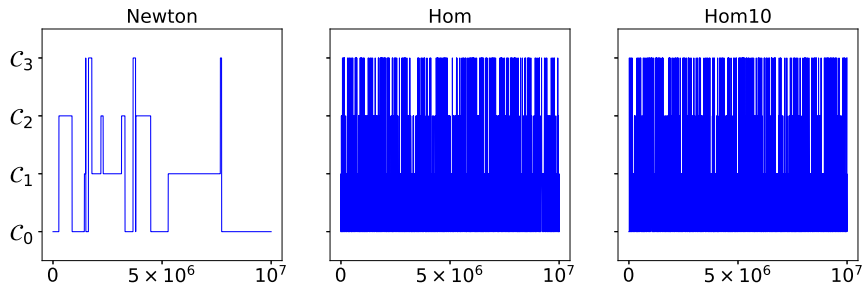


Figure 7: Sampling of the 9D sphere: visits along the trajectories of the connected components  $\mathcal{C}_i$  in (48) for  $0 \leq i \leq 3$ , as functions of the iteration index, using the schemes “Newton”, “Hom”, and “Hom10”. While data for all MCMC iterations are plotted for the “Newton” scheme, data are shown only every 5000 iterations for both “Hom” and “Hom10”, in order to have a good visual effect.

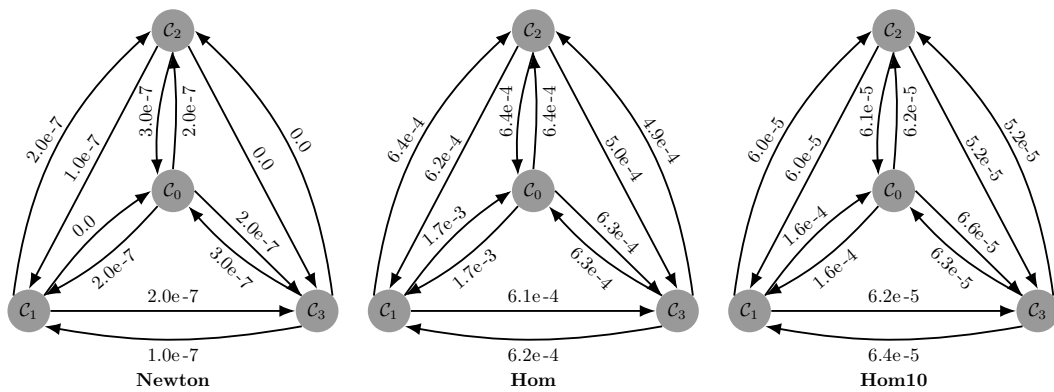


Figure 8: Sampling of the 9D sphere: graph representations of the transitions among the connected components  $\mathcal{C}_i$  for  $0 \leq i \leq 3$ . The frequencies of the transitions from one connected component  $\mathcal{C}_i$  to another component  $\mathcal{C}_j$  are shown on the edge from node  $i$  to  $j$ . The reported frequencies are empirical frequencies obtained on trajectories of  $N = 10^7$  iterations.

## 4 Proofs of the results presented in Section 2

### 4.1 Proofs of the results of Section 2.1

We prove Propositions 1 and 2, and then Theorem 1.

*Proof of Proposition 1.* Concerning the first item,  $G_x$  is clearly  $C^1$ -differentiable. Using the fact that, for all  $x \in \Sigma$ , the  $k$  columns of  $\nabla\xi(x)$  concatenated with the  $d - k$  columns of  $U_x$  form a basis in  $\mathbb{R}^d$  such that  $\nabla\xi(x)^T U_x = 0$ , we have, for all  $x, y \in \Sigma$ ,

$$\begin{aligned} \det(\nabla\xi(y)^T \nabla\xi(x)) = 0 &\iff \exists c \in \mathbb{R}^k \setminus \{0\}, \quad \nabla\xi(y)^T \nabla\xi(x)c = 0, \\ &\iff \exists(c, v) \in (\mathbb{R}^k \setminus \{0\}) \times (\mathbb{R}^{d-k} \setminus \{0\}), \quad \nabla\xi(x)c = U_y v, \\ &\iff \exists v \in \mathbb{R}^{d-k} \setminus \{0\}, \quad U_x^T U_y v = 0, \\ &\iff \det(U_x^T U_y) = 0, \end{aligned} \tag{49}$$

which implies that

$$C_x = \{y \in \Sigma \mid \det(\nabla\xi(y)^T \nabla\xi(x)) = 0\} = \{y \in \Sigma \mid \det(U_x^T U_y) = 0\}, \tag{50}$$

where the rightmost set in (50) is the set of critical points of  $G_x$ . Therefore, the differential of  $G_x$  has full rank at  $y \in \Sigma \setminus C_x$  and, as a result, there exists a neighborhood  $\mathcal{Q}$  of  $y$  such that  $G_x|_{\mathcal{Q}}$  is a  $C^1$ -diffeomorphism.

For the second item, it is clear that the function  $c(\cdot)$  in (7) is  $C^1$ -differentiable. Using the definition of  $F_x$  in (3), it is also straightforward to verify that it satisfies  $y = F_x(v, c(v))$ , as well as  $F_x(\bar{v}, c(\bar{v})) \in \mathcal{F}_x(\bar{v})$  for all  $\bar{v} \in G_x(\mathcal{Q})$ . Now assume that there exist a neighborhood  $\mathcal{O}$  of  $v$  and a  $C^1$ -differentiable function  $\tilde{c} : \mathcal{O} \rightarrow \mathbb{R}^k$  such that  $y = F_x(v, \tilde{c}(v))$  and  $F_x(\bar{v}, \tilde{c}(\bar{v})) \in \mathcal{F}_x(\bar{v})$  for all  $\bar{v} \in \mathcal{O}$ . Clearly, we have  $G_x(F_x(\bar{v}, \tilde{c}(\bar{v}))) = \bar{v}$  for all  $\bar{v} \in \mathcal{O} \cap G_x(\mathcal{Q})$ . Since  $G_x|_{\mathcal{Q}}$  is a  $C^1$ -diffeomorphism and  $F_x$  is defined in (3), we can directly compute  $\tilde{c}$  and obtain

$$\tilde{c}(\bar{v}) = (\nabla\xi^T(x) \nabla\xi(x))^{-1} \nabla\xi^T(x) ((G_x|_{\mathcal{Q}})^{-1}(\bar{v}) - x + \tau \nabla\bar{V}(x)), \quad \forall \bar{v} \in \mathcal{O} \cap G_x(\mathcal{Q}).$$

Therefore,  $\tilde{c}(\cdot)$  coincides with  $c(\cdot)$  on  $\mathcal{O} \cap G_x(\mathcal{Q})$ . This proves the assertion in the second item.  $\square$

*Proof of Proposition 2.* We first show that  $\mathcal{N}_x$  is closed and has zero Lebesgue measure. Since  $\Sigma$  is compact (Assumption 1), the set  $C_x$  in (6) is closed and the map  $G_x$  in (5) is continuous, a simple proof shows that the set  $\mathcal{N}_x$  is a closed subset of  $\mathbb{R}^{d-k}$ . Furthermore, (50) implies that  $C_x$  is in fact the set of critical values of  $G_x$ . As a result, Sard's theorem asserts that  $\mathcal{N}_x = G_x(C_x)$  is a subset of  $\mathbb{R}^{d-k}$  with Lebesgue measure zero [2]. This proves the assertion in the first item.

We next show that  $\mathcal{F}_x(v)$  is a finite set for any  $v \in \mathbb{R}^{d-k} \setminus \mathcal{N}_x$ . Assume by contradiction that there exists an element  $v \in \mathbb{R}^{d-k} \setminus \mathcal{N}_x$  for which this is not true. Then there are infinitely many Lagrange multipliers  $c_1, c_2, \dots \in \mathbb{R}^k$ , which are different from each other, such that  $F_x(v, c_i) = y^{(i)} \in \mathcal{F}_x(v) \subset \Sigma$ . Since  $\Sigma$  is compact, we can assume (upon extracting a subsequence) that  $\lim_{i \rightarrow +\infty} y^{(i)} = y \in \Sigma$ . Note that  $y^{(i)} - y^{(j)} = \nabla\xi(x)(c_i - c_j)$ . Using the fact that  $\nabla\xi(x)$  has full rank by Assumption 1, it holds

$$c_i - c_j = (\nabla\xi(x)^T \nabla\xi(x))^{-1} \nabla\xi(x)^T (y^{(i)} - y^{(j)}),$$

and so there exists  $c \in \mathbb{R}^k$  such that  $\lim_{i \rightarrow +\infty} c_i = c$  (since  $(c_i)_{i \geq 1}$  is a Cauchy sequence) and  $F_x(v, c) = y$ . Note that  $v = G_x(y) \in \mathbb{R}^{d-k} \setminus \mathcal{N}_x$  implies  $y \notin C_x$ . Therefore, by the first item of Proposition 1, we can find a neighborhood  $\mathcal{Q}$  of  $y$  such that  $G_x : \mathcal{Q} \rightarrow G_x(\mathcal{Q})$  is a  $C^1$ -diffeomorphism. However, this leads to a contradiction with the assumption that  $G_x(y^{(i)}) = v$  and  $\lim_{i \rightarrow +\infty} y^{(i)} = y$ , and so, the set  $\mathcal{F}_x(v)$  can contain at most a finite number of elements. This proves the assertion in the second item.

Concerning the third item, by Proposition 1, for each  $y^{(i)}$ ,  $1 \leq i \leq n$ , we can find a neighborhood  $\mathcal{Q}_i$  of  $y^{(i)}$  such that  $G_x|_{\mathcal{Q}_i}$  is a  $C^1$ -diffeomorphism. Assuming without loss of generality that  $\mathcal{Q}_i \cap \mathcal{Q}_{i'} = \emptyset$ , for  $1 \leq i \neq i' \leq n$ , Proposition 1 already implies that there are  $n$  different Lagrange multiplier functions  $c^{(i)}$ , locally given by (7) with  $\mathcal{Q} = \mathcal{Q}_i$ , and the set  $\mathcal{F}_x(\bar{v})$  has at least  $n$  elements for  $\bar{v}$  in the neighborhood  $\mathcal{O}$  of  $v$ , where  $\mathcal{O} = \cap_{i=1}^n G_x(\mathcal{Q}_i)$ . Suppose that  $\mathcal{F}_x(\bar{v})$  has  $n+1$  values or more for elements  $\bar{v} \in \mathcal{O}$  arbitrarily close to  $v$ . This means that we can find a sequence of configurations  $(\bar{y}^{(j)})_{j \geq 1} \subset \Sigma$  such that  $\bar{y}^{(j)} \notin \cup_{i=1}^n \mathcal{Q}_i$  and  $G_x(\bar{y}^{(j)}) = v_j \rightarrow v$  as  $j \rightarrow +\infty$ . It implies that  $G_x(y) = v$ , where  $y \notin \cup_{i=1}^n \mathcal{Q}_i$  is a limiting point of  $\bar{y}^{(j)}$  on  $\Sigma$  (obtained after a possible extraction). This is in contradiction with the fact that  $|\mathcal{F}_x(v)| = n$  and so, there exists a neighborhood  $\mathcal{O}' \subset \mathcal{O}$  of  $v$  such that  $\mathcal{F}_x(\bar{v})$  has exactly  $n$  values for any  $\bar{v}$  in  $\mathcal{O}'$ .

Finally, concerning the fourth item, we first note that  $\mathcal{N}_x \cap \mathcal{B}_{x,0} = \emptyset$  (indeed, if  $v \in \mathcal{N}_x$ , then there exists  $y \in C_x$  such that  $v = G_x(y)$ , so that  $|\mathcal{F}_x(v)| \geq 1$ , which implies that  $v \notin \mathcal{B}_{x,0}$ ). Since  $\mathcal{N}_x \cap \mathcal{B}_{x,i} = \emptyset$  by definition for  $i \geq 1$ , we can conclude that  $\mathcal{N}_x, \mathcal{B}_{x,0}, \mathcal{B}_{x,1}, \dots$  are disjoint subsets which form a partition of  $\mathbb{R}^{d-k}$ . The fact that  $\mathcal{B}_{x,0}$  is open can easily be shown by contradiction: Consider  $v \in \mathcal{B}_{x,0}$  and assume that there is a sequence  $(v_n) \subset \mathbb{R}^{d-k} \setminus \mathcal{B}_{x,0}$  such that  $v_n \rightarrow v$ ; in particular,  $v_n = G_x(y_n)$  for some  $y_n \in \Sigma$ ; then, up to extraction,  $y_n \rightarrow y$  so that  $v = G_x(y)$  and  $|\mathcal{F}_x(v)| \geq 1$  in contradiction with  $v \in \mathcal{B}_{x,0}$ .  $\square$

*Proof of Theorem 1.* This proof is adapted from [37]. For  $x \in \Sigma$ , we denote by  $\tilde{q}(x, \cdot)$  and  $q(x, \cdot)$  the probability distribution of the proposal state  $\tilde{x}^{(i+1)} \in \Sigma$  and the probability kernel of the Markov chain generated by Algorithm 1, respectively. We show that  $q$  satisfies the following detailed balance condition:

$$q(x, dy) e^{-\beta V(x)} \sigma_\Sigma(dx) = q(y, dx) e^{-\beta V(y)} \sigma_\Sigma(dy),$$

which should be understood as an equality in terms of measures in the product space  $\Sigma \times \Sigma$ . Recall the set  $\mathcal{D}$  defined in (12) and the acceptance probability  $a(y | x)$  defined in (17). According to Algorithm 1,  $q$  is given by

$$q(x, dy) = a(y | x) \mathbf{1}_{\mathcal{D}}(x, y) \tilde{q}(x, dy) + \left[ 1 - \int_{\Sigma} a(y' | x) \mathbf{1}_{\mathcal{D}}(x, y') \tilde{q}(x, dy') \right] \delta_x(dy), \quad (51)$$

where  $\mathbf{1}_{\mathcal{D}}$  is the indicator function of the set  $\mathcal{D}$  and  $\delta_x$  denotes the Dirac measure on  $\Sigma$  centered at  $x$ . Since  $x^{(i+1)}$  in Algorithm 1 is chosen randomly from the set  $\Psi_x(v)$ , with  $v \in \mathbb{R}^{d-k}$  following the Gaussian distribution (13), we know that  $\tilde{q}(x, \cdot)$  is the push-forward measure of (13) under the map  $\Psi_x$ . Moreover,  $\text{Im} \Psi_x \cap C_x \subset \Psi_x(\mathcal{N}_x)$  and  $\mathcal{N}_x$  has zero measure under the Gaussian distribution in (13), which implies that  $\tilde{q}(x, \text{Im} \Psi_x \cap C_x) = \tilde{q}(x, \Psi_x(\mathcal{N}_x)) = 0$ . Also, given any  $y \in \text{Im} \Psi_x$ , the element  $v$  is determined by (5) and therefore (11) is satisfied. In view of



Assumption 2, we can apply the formula of the push-forward measures given in [1, Lemma 5.5.3] and a localization argument similar to the one discussed at the end of the proof of Theorem 2 to obtain

$$\tilde{q}(x, dy) = \begin{cases} \frac{\omega(y | x, v)}{|\det D\Psi_x^{(j)}(v)|} \left(\frac{2\pi}{\beta}\right)^{-\frac{d-k}{2}} e^{-\frac{\beta|v|^2}{2}} \sigma_\Sigma(dy), & y \in \text{Im}\Psi_x \setminus C_x \text{ and } y \in \Psi_x(v), \\ 0, & \text{otherwise,} \end{cases} \quad (52)$$

where  $\Psi_x^{(j)}$  is the map in Assumption 2 such that  $y = \Psi_x^{(j)}(v)$ . Note that the value of the index  $j \in \{1, \dots, m\}$  is not essential and in fact we have  $\Psi_x^{(j)} = (G_x|_{\mathcal{Q}})^{-1}$ , where  $\mathcal{Q}$  is a neighborhood of  $y$  such that  $G_x|_{\mathcal{Q}}$  is a  $C^1$ -diffeomorphism.

Let us define the set

$$\tilde{\mathcal{D}} = \{(x, y) \in \Sigma \times \Sigma \mid y \in \text{Im}\Psi_x, x \in \text{Im}\Psi_y, \det(\nabla\xi(y)^T \nabla\xi(x)) \neq 0\}. \quad (53)$$

Since  $\tilde{q}(x, \text{Im}\Psi_x \cap C_x) = 0$  for any  $x \in \Sigma$ , the set  $\tilde{\mathcal{D}}$  differs from  $\mathcal{D}$  by a set that has zero measure under the product measure  $\sigma_\Sigma(dx)\tilde{q}(x, dy)$ . Using this fact, as well as (51), we can compute

$$\begin{aligned} \int_{\Sigma \times \Sigma} f(x, y) q(x, dy) e^{-\beta V(x)} \sigma_\Sigma(dx) &= \int_{\Sigma \times \Sigma} f(x, y) a(y | x) \mathbf{1}_{\tilde{\mathcal{D}}}(x, y) e^{-\beta V(x)} \sigma_\Sigma(dx) \tilde{q}(x, dy) \\ &+ \int_{\Sigma} f(x, x) \left[ 1 - \int_{\Sigma} a(y' | x) \mathbf{1}_{\tilde{\mathcal{D}}}(x, y') \tilde{q}(x, dy') \right] e^{-\beta V(x)} \sigma_\Sigma(dx). \end{aligned} \quad (54)$$

Now, for  $(x, y) \in \tilde{\mathcal{D}}$ , we denote by  $v' = G_y(x) \in \mathbb{R}^{d-k}$  the unique element such that  $x \in \Psi_y(v')$ . Since  $(x, y) \in \tilde{\mathcal{D}}$  implies  $x \notin C_y$ , thanks to Assumption 2, there exists a  $C^1$ -diffeomorphism  $\Psi_y^{(j')}$  with  $x = \Psi_y^{(j')}(v')$ . Again, the value of the index  $j'$  is not essential since in fact  $\Psi_y^{(j')} = (G_y|_{\mathcal{Q}'})^{-1}$ , where  $\mathcal{Q}'$  is a neighborhood of  $x$  such that  $G_y|_{\mathcal{Q}'}$  is a  $C^1$ -diffeomorphism.

The choice

$$\forall (x, y) \in \tilde{\mathcal{D}}, a(y | x) = \min \left\{ 1, \frac{\omega(x | y, v') |\det D\Psi_x^{(j)}(v)|}{\omega(y | x, v) |\det D\Psi_y^{(j')}(v')|} e^{-\beta[(V(y) + \frac{1}{2}|v'|^2) - (V(x) + \frac{1}{2}|v|^2)]} \right\} \quad (55)$$

then implies with (52) that

$$\begin{aligned} \int_{\Sigma \times \Sigma} f(x, y) a(y | x) \mathbf{1}_{\tilde{\mathcal{D}}}(x, y) e^{-\beta V(x)} \sigma_\Sigma(dx) \tilde{q}(x, dy) \\ = \int_{\Sigma \times \Sigma} f(x, y) a(x | y) \mathbf{1}_{\tilde{\mathcal{D}}}(x, y) e^{-\beta V(y)} \sigma_\Sigma(dy) \tilde{q}(y, dx). \end{aligned} \quad (56)$$

The equalities (54) and (56) plus the fact that  $\mathbf{1}_{\tilde{\mathcal{D}}}$  is symmetric in turn imply (18). Moreover, using the facts that  $\Psi_x^{(j)} = (G_x|_{\mathcal{Q}})^{-1}$  and  $\Psi_y^{(j')} = (G_y|_{\mathcal{Q}'})^{-1}$ , as well as the definition of  $G_x$  in (5), we can compute

$$\det D\Psi_x^{(j)}(v) = \det D(G_x|_{\mathcal{Q}})^{-1}(v) = \frac{1}{\det D(G_x|_{\mathcal{Q}})(y)} = (2\tau)^{\frac{d-k}{2}} \det(U_x^T U_y)^{-1}$$

$$= \frac{1}{\det D(G_y|_{\mathcal{Q}'}) (x)} = \det D(G_y|_{\mathcal{Q}})^{-1}(v') = \det D\Psi_y^{(j')}(v').$$

Therefore, (55) reduces to the acceptance probability (17). This allows to conclude that the Markov chain generated by Algorithm 1 is indeed reversible with respect to  $\nu$  on  $\Sigma$ .  $\square$

## 4.2 Proofs of the results of Section 2.2

We prove Propositions 3 and 4, then Lemma 2, and finally Theorem 2.

*Proof of Proposition 3.* The proof of Proposition 3 is similar to the proof of Proposition 1. First of all, for a given  $x \in \Sigma$ , with an argument similar to the one used to write (49), we can verify that

$$C_{M,x} = \{y \in \Sigma \mid \det(\nabla\xi(y)^T M^{-1} \nabla\xi(x)) = 0\} = \{y \in \Sigma \mid \det(U_{M,x}^T M^{-1} U_{M,y}) = 0\}. \quad (57)$$

Therefore,  $C_{M,x}$  is the set of critical points of the map  $G_{M,x}$  defined in (31).

The first item can be obtained by applying the implicit function theorem to the equation  $g(\bar{z}, y) = 0$  starting from the solution  $g(z, x^1) = 0$ , where the map  $g : T^*\Sigma \times \Sigma \rightarrow \mathbb{R}^{d-k}$ , defined as  $g(\bar{z}, y) = U_{M,\bar{x}}^T M^{-1}(G_{M,\bar{x}}(y) - \bar{p})$  for  $\bar{z} = (\bar{x}, \bar{p}) \in T^*\Sigma$  and  $y \in \Sigma$ , is  $C^1$ -differentiable, since  $U_{M,\bar{x}} \in \mathbb{R}^{d \times (d-k)}$  can be chosen in such a way that it is locally  $C^1$ -differentiable with respect to  $\bar{x}$ . In fact, using the definition of  $G_{M,x}$  in (31), we have

$$g(\bar{z}, y) = U_{M,\bar{x}}^T M^{-1}(G_{M,\bar{x}}(y) - \bar{p}) = \frac{1}{\tau} U_{M,\bar{x}}^T \left( y - \bar{x} + \frac{\tau^2}{2} M^{-1} \nabla \bar{V}(\bar{x}) - \tau M^{-1} \bar{p} \right).$$

A simple computation shows that the differential of  $g$  in the  $y$ -variable is invertible, which allows to express  $y$  as a  $C^1$  function of  $\bar{z}$ . This proves the first item.

Concerning the second item, using the facts that  $\Upsilon_1(z) = x^1$  and  $G_{M,\bar{x}}(\Upsilon_1(\bar{z})) = \bar{p}$  for all  $\bar{z} = (\bar{x}, \bar{p}) \in \mathcal{O}$ , as well as (28), (30) and (31), one can verify the claim regarding the Lagrange multiplier functions in (34) by direct computations. The uniqueness of the Lagrange multiplier  $\lambda_x$  follows from the uniqueness of the function  $\Upsilon_1$  as a solution in  $y$  to the implicit equation  $g(\bar{z}, y) = 0$ , while the uniqueness of  $\lambda_p$  is due to the fact that  $\lambda_p$  is determined once  $\lambda_x$  is given (see (30)). This proves the second item.

For the third item, note that the map  $\Upsilon = F(\cdot, \lambda_x(\cdot), \lambda_p(\cdot))$ , where the Lagrange multiplier functions are given in (34), is the one-step RATTLE with momentum reversal. The symplecticity of the RATTLE scheme (see [20] and [14, Section VII.1.4]) implies that  $|\det D\Upsilon| \equiv 1$ . Using this fact, we can find a neighborhood  $\mathcal{O}$  of  $z$  such that  $\Upsilon$  is a  $C^1$ -diffeomorphism on  $\mathcal{O}$ .  $\square$

*Proof of Proposition 4.* The proof of Proposition 4 is similar to the proof of Proposition 2.

Let us first show that  $\mathcal{N}$  is a closed set with zero Lebesgue measure. For a sequence  $(x^{(i)}, p^{(i)})$  in  $\mathcal{N}$  which converges to  $(x, p) \in T^*\Sigma$ , there exists  $y^{(i)} \in C_{M,x^{(i)}}$  such that  $p^{(i)} = G_{M,x^{(i)}}(y^{(i)})$ , where  $G_{M,x}$  is the map defined in (31). Since  $\Sigma$  is compact,  $y^{(i)}$  converges upon extraction to  $y \in \Sigma$ . Note that  $y \in C_{M,x}$ , since

$$\det(\nabla\xi(y)^T M^{-1} \nabla\xi(x)) = \lim_{i \rightarrow +\infty} \det(\nabla\xi(y^{(i)})^T M^{-1} \nabla\xi(x^{(i)})) = 0,$$

and that  $p = G_{M,x}(y)$ . This implies that  $(x, p) \in \mathcal{N}$  and therefore  $\mathcal{N}$  is a closed set. Also, as shown in the proof of Proposition 3 (see (57)),  $C_{M,x}$  is the set of critical points of the map  $G_{M,x}$ . As a result,  $\mathcal{N} \subset T^*\Sigma$  has zero Lebesgue measure in  $T^*\Sigma$ , since Sard's theorem implies that  $G_{M,x}(C_{M,x})$  has zero Lebesgue measure in  $T_x^*\Sigma$  for all  $x \in \Sigma$ . The equality (35) follows directly from the definitions of the set  $C_{M,x}$  in (33) and the map  $G_{M,x}$  in (31). This proves the assertion in the first item.

Concerning the second item, for any  $z = (x, p) \in T^*\Sigma \setminus \mathcal{N}$ , we can show that the set  $\mathcal{F}(z)$  contains at most a finite number of elements, by using an argument similar to the one used in the proof of the second item of Proposition 2, together with the first item of Proposition 3.

Concerning the third item, assuming that  $z = (x, p) \in T^*\Sigma \setminus \mathcal{N}$  and  $\mathcal{F}(z) = \{z^{(1)}, z^{(2)}, \dots, z^{(n)}\}$  with  $n = |\mathcal{F}(z)| \geq 1$ , the third assertion of Proposition 3 implies that we can find a neighborhood  $\mathcal{O}$  of  $z$  and  $n$  different pairs of Lagrange multiplier functions  $\lambda_x^{(i)}, \lambda_p^{(i)} : \mathcal{O} \rightarrow \mathbb{R}^k$ ,  $1 \leq i \leq n$ , such that  $\Upsilon^{(i)}(\cdot) = F(\cdot, \lambda_x^{(i)}(\cdot), \lambda_p^{(i)}(\cdot))$  is a  $C^1$ -diffeomorphism from  $\mathcal{O}$  to a neighborhood of  $z^{(i)}$  in  $T^*\Sigma$ . Using this fact and repeating the argument in the proof of the third item of Proposition 2 (considering the position variable), we can again show by contradiction that there exists a neighborhood  $\mathcal{O}$  of  $z$  such that the set  $\mathcal{F}(\bar{z})$  has exactly  $n$  elements  $\Upsilon^{(1)}(\bar{z}), \Upsilon^{(2)}(\bar{z}), \dots, \Upsilon^{(n)}(\bar{z})$  for all  $\bar{z} \in \mathcal{O}$ .

Concerning the fourth item, the third item above implies that the subsets  $\mathcal{B}_i$  are open for  $i \geq 1$ . By proceeding in the same way as at the end of the proof of Proposition 2, it is easy to show by contradiction that  $\mathcal{B}_0$  is open, and that  $\mathcal{N}, \mathcal{B}_0, \mathcal{B}_1, \dots$  are disjoint subsets which form a partition of  $T^*\Sigma$ .  $\square$

*Proof of Lemma 2.* Denote by  $\tilde{q}(z, dz')$  the transition probability kernel of the Markov chain  $\tilde{\mathcal{E}}$ . Then,  $\tilde{q}(z, \cdot) = \mathcal{R}_\#(q(z, \cdot))$  for  $z \in T^*\Sigma$ , where  $\mathcal{R}_\#(q(z, \cdot))$  denotes the push-forward probability measure of  $q(z, \cdot)$  by the involution map  $\mathcal{R}$ . Assume that the Markov chain  $\mathcal{E}$  is reversible. Using the change of variables formula for the push-forward measures [1, Section 5.2], as well as  $\mathcal{R} \circ \mathcal{R} = \text{id}$ , it holds, for any bounded continuous function  $f : T^*\Sigma \times T^*\Sigma \rightarrow \mathbb{R}$ ,

$$\begin{aligned} \int_{T^*\Sigma \times T^*\Sigma} f(z, z') \tilde{q}(z, dz') \mu(dz) &= \int_{T^*\Sigma \times T^*\Sigma} f(z, z') \mathcal{R}_\#(q(z, \cdot))(dz') \mu(dz) \\ &= \int_{T^*\Sigma \times T^*\Sigma} f(z, \mathcal{R}(z')) q(z, dz') \mu(dz) \\ &= \int_{T^*\Sigma \times T^*\Sigma} f(z', \mathcal{R}(z)) q(z, dz') \mu(dz) \\ &= \int_{T^*\Sigma \times T^*\Sigma} f(\mathcal{R}(z'), \mathcal{R}(z)) \mathcal{R}_\#(q(z, \cdot))(dz') \mu(dz) \\ &= \int_{T^*\Sigma \times T^*\Sigma} f(\mathcal{R}(z'), \mathcal{R}(z)) \tilde{q}(z, dz') \mu(dz), \end{aligned}$$

which shows that the Markov chain  $\tilde{\mathcal{E}}$  is reversible up to momentum reversal. The proof of the converse statement (*i.e.*  $\mathcal{E}$  is reversible if  $\tilde{\mathcal{E}}$  is reversible up to momentum reversal) is similar and is therefore omitted.  $\square$

*Proof of Theorem 2.* Let us denote by  $\mathcal{E}$  the Markov chain in Algorithm 2 which corresponds to the transition from  $z^{(i)}$  to  $z^{(i+1)}$ , and denote by  $q(z, dz')$  its transition probability kernel. We prove that  $\mathcal{E}$  is reversible up to momentum reversal by considering it as the composition of the

transitions (in Algorithm 2) from  $z^{(i)}$  to  $z^{(i+\frac{1}{4})}$ , then from  $z^{(i+\frac{1}{4})}$  to  $z^{(i+\frac{3}{4})}$ , and finally from  $z^{(i+\frac{3}{4})}$  to  $z^{(i+1)}$ .

Denote by  $q_1, q_2, \tilde{q}_2$  the transition probability kernels which correspond to the transitions from  $z^{(i)}$  to  $z^{(i+\frac{1}{4})}$ , from  $z^{(i+\frac{1}{4})}$  to  $z^{(i+\frac{2}{4})}$ , and from  $z^{(i+\frac{1}{4})}$  to  $z^{(i+\frac{3}{4})}$ , respectively. Denote also by  $\mathcal{C}_1, \mathcal{C}_2, \tilde{\mathcal{C}}_2$  the corresponding Markov chains. The transition probability kernel  $q$  of the whole Markov chain  $\mathcal{C}$  is then obtained as the composition of the transition probability kernels of the Markov chains  $\mathcal{C}_1, \tilde{\mathcal{C}}_2, \mathcal{C}_1$ , *i.e.*

$$q(z, dz') = \int_{(z_1, z_2) \in T^*\Sigma \times T^*\Sigma} q_1(z, dz_1) \tilde{q}_2(z_1, dz_2) q_1(z_2, dz'), \quad z, z' \in T^*\Sigma. \quad (58)$$

Recall the definition of reversibility in Definition 1 and the definition of reversibility up to momentum reversal in Definition 2. We state the following two claims (C1)–(C2):

(C1) The Markov chain  $\mathcal{C}_1$  is both reversible and reversible up to momentum reversal with respect to  $\mu$ .

(C2) The Markov chain  $\tilde{\mathcal{C}}_2$  is reversible up to momentum reversal with respect to  $\mu$ .

Also, since  $\tilde{\mathcal{C}}_2$  is the Markov chain  $\mathcal{C}_2$  followed by momentum reversal, Lemma 2 implies that Claim (C2) is equivalent to the following claim:

(C2') The Markov chain  $\mathcal{C}_2$  is reversible with respect to  $\mu$ .

Let us first show that the fact that the whole Markov chain  $\mathcal{C}$  is reversible up to momentum reversal with respect to  $\mu$  is a consequence of Claims (C1)–(C2). In fact, using (58), Fubini's theorem, and the invariance of  $\mu$  under  $\mathcal{R}$ , we obtain, for any bounded continuous function  $f : T^*\Sigma \times T^*\Sigma \rightarrow \mathbb{R}$ ,

$$\begin{aligned} & \int_{T^*\Sigma \times T^*\Sigma} f(z, z') q(z, dz') \mu(dz) \\ &= \int_{T^*\Sigma \times T^*\Sigma \times T^*\Sigma \times T^*\Sigma} f(z, z') q_1(z, dz_1) \tilde{q}_2(z_1, dz_2) q_1(z_2, dz') \mu(dz) \\ &= \int_{T^*\Sigma \times T^*\Sigma \times T^*\Sigma \times T^*\Sigma} f(\mathcal{R}(z_1), z') q_1(z, dz_1) \tilde{q}_2(\mathcal{R}(z), dz_2) q_1(z_2, dz') \mu(dz) \\ &= \int_{T^*\Sigma \times T^*\Sigma \times T^*\Sigma \times T^*\Sigma} f(\mathcal{R}(z_1), z') q_1(\mathcal{R}(z), dz_1) \tilde{q}_2(z, dz_2) q_1(z_2, dz') \mu(dz) \\ &= \int_{T^*\Sigma \times T^*\Sigma \times T^*\Sigma \times T^*\Sigma} f(\mathcal{R}(z_1), z') q_1(z_2, dz_1) \tilde{q}_2(z, dz_2) q_1(\mathcal{R}(z), dz') \mu(dz) \\ &= \int_{T^*\Sigma \times T^*\Sigma \times T^*\Sigma \times T^*\Sigma} f(\mathcal{R}(z_1), z') q_1(z_2, dz_1) \tilde{q}_2(\mathcal{R}(z), dz_2) q_1(z, dz') \mu(dz) \\ &= \int_{T^*\Sigma \times T^*\Sigma \times T^*\Sigma \times T^*\Sigma} f(\mathcal{R}(z_1), \mathcal{R}(z)) q_1(z_2, dz_1) \tilde{q}_2(z', dz_2) q_1(z, dz') \mu(dz) \\ &= \int_{T^*\Sigma \times T^*\Sigma} f(\mathcal{R}(z'), \mathcal{R}(z)) q(z, dz') \mu(dz), \end{aligned}$$

where we applied successively: the reversibility up to momentum reversal on  $(z, z_1)$  (thanks to Claim (C1)); a change of variable from  $z$  to  $\mathcal{R}(z)$ ; the reversibility up to momentum reversal

on  $(z, z_2)$  (thanks to Claim (C2)); a change of variable from  $z$  to  $\mathcal{R}(z)$ ; the reversibility up to momentum reversal on  $(z, z')$  (thanks to Claim (C1)).

We conclude by proving Claim (C1) and Claim (C2'); starting with (C1). Note that, in view of (25) and (39), it holds, for  $z = (x, p), z' = (x', p') \in T^*\Sigma$ ,

$$q_1(z, dz') = \left( \frac{2\pi(1-\alpha^2)}{\beta} \right)^{-\frac{d-k}{2}} \exp \left( -\frac{\beta(p' - \alpha p)^T M^{-1}(p' - \alpha p)}{2(1-\alpha^2)} \right) \sigma_{T_x^*\Sigma}^{M^{-1}}(dp') \delta_x(dx'). \quad (59)$$

Therefore, using (23), (25) and (59), we can compute

$$q_1(z, dz') \mu(dz) = \left( \frac{2\pi(1-\alpha^2)}{\beta} \right)^{k-d} \exp \left( -\frac{\beta(\langle p', p' \rangle_{M^{-1}} - 2\alpha \langle p, p' \rangle_{M^{-1}} + \langle p, p \rangle_{M^{-1}})}{2(1-\alpha^2)} \right) \times \sigma_{T_x^*\Sigma}^{M^{-1}}(dp') \sigma_{T_x^*\Sigma}^{M^{-1}}(dp) \delta_x(dx') \nu_M(dx), \quad (60)$$

where  $\nu_M$  is defined in (24) and  $\langle \cdot, \cdot \rangle_{M^{-1}}$  is defined in (21). Using (60), it is straightforward to verify that, for any bounded continuous function  $f : T^*\Sigma \times T^*\Sigma \rightarrow \mathbb{R}$ ,

$$\begin{aligned} \int_{T^*\Sigma \times T^*\Sigma} f(z, z') q_1(z, dz') \mu(dz) &= \int_{T^*\Sigma \times T^*\Sigma} f(z', z) q_1(z, dz') \mu(dz) \\ &= \int_{T^*\Sigma \times T^*\Sigma} f(\mathcal{R}(z'), \mathcal{R}(z)) q_1(z, dz') \mu(dz), \end{aligned} \quad (61)$$

This shows that  $\mathcal{C}_1$  is both reversible and reversible up to a momentum reversal with respect to  $\mu$ . Therefore, Claim (C1) is proved.

It remains to prove Claim (C2'). According to Algorithm 2, we have

$$\begin{aligned} q_2(z, dz') &= \sum_{j=1}^{|\Phi(z)|} \omega(z_j | z) \mathbf{1}_{\mathcal{D}_\Phi}(z, z_j) a(z_j | z) \delta_{z_j}(dz') \\ &\quad + \left[ 1 - \sum_{j=1}^{|\Phi(z)|} \omega(z_j | z) \mathbf{1}_{\mathcal{D}_\Phi}(z, z_j) a(z_j | z) \right] \delta_z(dz'), \end{aligned} \quad (62)$$

where  $\mathcal{D}_\Phi$  is the set defined in (38),  $\Phi(z) = \{z_1, \dots, z_n\}$ , with  $n = |\Phi(z)|$ ,  $a(\cdot | z)$  is the acceptance probability in (40), and  $\delta_z$  the Dirac measure centered at  $z \in T^*\Sigma$ . Here and in the following, we adopt the convention that  $\sum_{j=1}^0 \cdot = 0$ . Let us show that, for any bounded measurable function  $f : T^*\Sigma \times T^*\Sigma \rightarrow \mathbb{R}$ ,

$$\int_{(T^*\Sigma)^2} f(z, z') q_2(z, dz') e^{-\beta H(z)} \sigma_{T^*\Sigma}(dz) = \int_{(T^*\Sigma)^2} f(z', z) q_2(z, dz') e^{-\beta H(z)} \sigma_{T^*\Sigma}(dz). \quad (63)$$

Using (62), the integral on the left hand side above can be written as

$$\int_{T^*\Sigma \times T^*\Sigma} f(z, z') q_2(z, dz') e^{-\beta H(z)} \sigma_{T^*\Sigma}(dz) = I_1 + I_2,$$

with

$$I_1 = \int_{T^*\Sigma} \left[ \sum_{j=1}^{|\Phi(z)|} \omega(z_j | z) \mathbf{1}_{\mathcal{D}_\Phi}(z, z_j) a(z_j | z) f(z, z_j) \right] e^{-\beta H(z)} \sigma_{T^*\Sigma}(dz),$$

$$I_2 = \int_{T^*\Sigma} \left[ 1 - \sum_{j=1}^{|\Phi(z)|} \omega(z_j | z) \mathbf{1}_{\mathcal{D}_\Phi}(z, z_j) a(z_j | z) \right] f(z, z) e^{-\beta H(z)} \sigma_{T^*\Sigma}(dz).$$

The expression of the acceptance probability in (40) implies that

$$I_1 = \int_{T^*\Sigma} \left[ \sum_{z' \in \Phi(z)} \min \left\{ \omega(z' | z) e^{-\beta H(z)}, \omega(z | z') e^{-\beta H(z')} \right\} \mathbf{1}_{\mathcal{D}_\Phi}(z, z') f(z, z') \right] \sigma_{T^*\Sigma}(dz).$$

In the same way, the integral on the right hand side of (63) can be written as the sum of  $\tilde{I}_1$  and  $I_2$ , where

$$\tilde{I}_1 = \int_{T^*\Sigma} \left[ \sum_{z' \in \Phi(z)} \min \left\{ \omega(z' | z) e^{-\beta H(z)}, \omega(z | z') e^{-\beta H(z')} \right\} \mathbf{1}_{\tilde{\mathcal{D}}_\Phi}(z, z') f(z', z) \right] \sigma_{T^*\Sigma}(dz).$$

Therefore, it suffices to prove that  $I_1 = \tilde{I}_1$ .

To proceed, recall that  $\Pi$  is the projection map defined in (37). As stated in Assumption 3, we assume that the first  $m$  elements  $z_1, \dots, z_m$  in  $\Phi(z)$ , where  $0 \leq m \leq |\Phi(z)|$ , satisfy  $\Pi(z_j) \in \Sigma \setminus C_{M, \Pi(z)}$  for  $j \leq m$ . We write  $m(z)$  in the sequel in order to emphasize the dependence on  $z$ . Let us introduce the set

$$\tilde{\mathcal{D}}_\Phi = \left\{ (z, z') \in T^*\Sigma \times T^*\Sigma \mid z' \in \Phi(z), z \in \Phi(z'), \right. \\ \left. \det [\nabla \xi(\Pi(z'))^T M^{-1} \nabla \xi(\Pi(z))] \neq 0 \right\}, \quad (64)$$

which is a subset of the set  $\mathcal{D}_\Phi$  defined in (38). It will play a role similar to the set  $\tilde{\mathcal{D}}$  defined in (53).

Note that, if  $z_j \in \Phi(z)$  and  $\Pi(z_j) \in C_{M, \Pi(z)}$  for some  $1 \leq j \leq |\Phi(z)|$ , then  $z \in \mathcal{N}$ . Therefore,  $\mathbf{1}_{\mathcal{D}_\Phi}(z, z_j) = \mathbf{1}_{\tilde{\mathcal{D}}_\Phi}(z, z_j)$ , except for  $z$  in the zero measure set  $\mathcal{N}$  (Proposition 4). Also,  $\mathbf{1}_{\tilde{\mathcal{D}}_\Phi}(z, z_j) = 0$  when  $m(z) < j \leq |\Phi(z)|$ . Using these facts, we can compute

$$I_1 = \int_{T^*\Sigma} \left[ \sum_{z' \in \Phi(z)} \min \left\{ \omega(z' | z) e^{-\beta H(z)}, \omega(z | z') e^{-\beta H(z')} \right\} \mathbf{1}_{\tilde{\mathcal{D}}_\Phi}(z, z') f(z, z') \right] \sigma_{T^*\Sigma}(dz)$$

$$= \int_{T^*\Sigma} \left[ \sum_{j=1}^{m(z)} \min \left\{ \omega(\Phi^{(j)}(z) | z) e^{-\beta H(z)}, \omega(z | \Phi^{(j)}(z)) e^{-\beta H(\Phi^{(j)}(z))} \right\} \right. \\ \left. \times \mathbf{1}_{\tilde{\mathcal{D}}_\Phi}(z, \Phi^{(j)}(z)) f(z, \Phi^{(j)}(z)) \right] \sigma_{T^*\Sigma}(dz), \quad (65)$$

where  $\Phi^{(j)}$  are the maps considered in Assumption 3.

The idea now is to consider the preimages  $z$  of a fixed  $z' = \Phi^{(j)}(z) \in T^*\Sigma$  in (65). Note

that, by the definition of the set  $\widetilde{\mathcal{D}}_\Phi$  in (64), it is apparent that, for all  $z, z' \in T^*\Sigma$ ,

$$\mathbf{1}_{\widetilde{\mathcal{D}}_\Phi}(z, z') = 1 \iff \mathbf{1}_{\widetilde{\mathcal{D}}_\Phi}(z', z) = 1. \quad (66)$$

This implies that any preimage  $z$  of  $z'$  such that  $\mathbf{1}_{\widetilde{\mathcal{D}}_\Phi}(z, z') = 1$  is given by the image  $\bar{z}_j = \Phi^{(j)}(z')$ , for some  $1 \leq j \leq m(z')$ . Therefore, we can rewrite (65) as

$$I_1 = \int_{T^*\Sigma} \left[ \sum_{j=1}^{m(z')} \min \left\{ \omega(z' | \bar{z}_j) e^{-\beta H(\bar{z}_j)}, \omega(\bar{z}_j | z') e^{-\beta H(z')} \right\} \mathbf{1}_{\widetilde{\mathcal{D}}_\Phi}(\bar{z}_j, z') f(\bar{z}_j, z') \right] \sigma_{T^*\Sigma}(dz').$$

Here, we have used the fact that  $\Phi^{(j)}$  is (locally)  $C^1$ -diffeomorphism and  $|\det(D\Phi^{(j)})| \equiv 1$  (see Assumption 3 and the third item of Proposition 3). This equality can for instance be obtained by a localization argument, where we first prove the equality for functions  $f(z, z')$  which are tensor products of indicator functions of small open sets in the variables  $z, z'$  (so that there is at most one image and one preimage) and then concluding by a density argument. Then,

$$\begin{aligned} I_1 &= \int_{T^*\Sigma} \left[ \sum_{\bar{z} \in \Phi(z')} \min \left\{ \omega(z' | \bar{z}) e^{-\beta H(\bar{z})}, \omega(\bar{z} | z') e^{-\beta H(z')} \right\} \mathbf{1}_{\widetilde{\mathcal{D}}_\Phi}(\bar{z}, z') f(\bar{z}, z') \right] \sigma_{T^*\Sigma}(dz') \\ &= \int_{T^*\Sigma} \left[ \sum_{\bar{z} \in \Phi(z')} \min \left\{ \omega(z' | \bar{z}) e^{-\beta H(\bar{z})}, \omega(\bar{z} | z') e^{-\beta H(z')} \right\} \mathbf{1}_{\mathcal{D}_\Phi}(\bar{z}, z') f(\bar{z}, z') \right] \sigma_{T^*\Sigma}(dz') \\ &= \widetilde{I}_1. \end{aligned}$$

In the above series of equalities, we used the fact that  $\mathbf{1}_{\widetilde{\mathcal{D}}_\Phi}(\bar{z}_j, z') = 0$ , for  $m(z') < j \leq |\Phi(z')|$  to derive the second equality, and that  $\mathbf{1}_{\mathcal{D}_\Phi}(\bar{z}, z') = \mathbf{1}_{\widetilde{\mathcal{D}}_\Phi}(\bar{z}, z')$ , except for  $z'$  in the zero measure set  $\mathcal{N}$  (Proposition 4), to derive the third equality. This completes the proof of Claim (C2').  $\square$

**Acknowledgements.** This study was inspired by the work of Paul Breiding and Orlando Marigliano [4]. The authors thank them both for fruitful discussions on the computations of multiple projections on submanifolds. WZ is funded by the Deutsche Forschungsgemeinschaft (DFG, German Research Foundation) under Germany's Excellence Strategy — The Berlin Mathematics Research Center MATH+ (EXC-2046/1, project ID: 390685689). TL and GS have received funding from the European Research Council (ERC) under the European Union's Horizon 2020 research and innovation programme (grant agreement No 810367). TL and GS also benefited from the scientific environment of the Laboratoire International Associé between the Centre National de la Recherche Scientifique and the University of Illinois at Urbana-Champaign. Finally, part of this work was done while TL was visiting the CNRS-ICL International Research Laboratory. TL would like to thank the Department of Mathematics at Imperial College of London for its hospitality.

## References

- [1] L. Ambrosio, N. Gigli, and G. Savaré. *Gradient Flows: In Metric Spaces and in the Space of Probability Measures*. Lectures in Mathematics. Birkhäuser, 2005.

- [2] A. Banyaga and D. Hurtubise. *Lectures on Morse Homology*. Texts in the Mathematical Sciences. Springer Netherlands, 2004.
- [3] D. J. Bates, J. D. Hauenstein, A. J. Sommese, and C. W. Wampler. Bertini: Software for numerical algebraic geometry. Available at [bertini.nd.edu](http://bertini.nd.edu) with permanent doi: [dx.doi.org/10.7274/R0H41PB5](https://doi.org/10.7274/R0H41PB5).
- [4] P. Breiding and O. Marigliano. Random points on an algebraic manifold. *arXiv preprint*, 1810.06271, 2018.
- [5] P. Breiding and S. Timme. Homotopycontinuation.jl: A package for homotopy continuation in Julia. In J. H. Davenport, M. Kauers, G. Labahn, and J. Urban, editors, *Mathematical Software – ICMS 2018*, pages 458–465, Cham, 2018. Springer International Publishing.
- [6] M. Brubaker, M. Salzmann, and R. Urtasun. A family of MCMC methods on implicitly defined manifolds. In N. D. Lawrence and M. Girolami, editors, *Proceedings of the Fifteenth International Conference on Artificial Intelligence and Statistics*, volume 22 of *Proceedings of Machine Learning Research*, pages 161–172. PMLR, 2012.
- [7] E. Cancès, F. Legoll, and G. Stoltz. Theoretical and numerical comparison of some sampling methods for molecular dynamics. *ESAIM: Math. Model. Num.*, 41(2):351–389, 2007.
- [8] S. Duane, A. Kennedy, B. J. Pendleton, and D. Roweth. Hybrid Monte Carlo. *Physics Letters B*, 195(2):216–222, 1987.
- [9] A. Durmus, E. Moulines, and E. Saksman. On the convergence of Hamiltonian Monte Carlo. *arXiv preprint*, 1705.00166, 2017.
- [10] Y. Fang, J. M. Sanz-Serna, and R. D. Skeel. Compressible generalized hybrid Monte Carlo. *J. Chem. Phys.*, 140(17):174108, 2014.
- [11] C. W. Gardiner. *Handbook of Stochastic Methods for Physics, Chemistry and the Natural Sciences*, volume 13 of *Springer Series in Synergetics*. Springer-Verlag, Berlin, third edition, 2004.
- [12] M. Girolami and B. Calderhead. Riemann manifold Langevin and Hamiltonian Monte Carlo methods. *J. R. Stat. Soc. Series B (Stat. Methodol.)*, 73(2):123–214, 2011.
- [13] M. Graham. MICI package. <https://github.com/matt-graham/mici>.
- [14] E. Hairer, C. Lubich, and G. Wanner. *Geometric Numerical Integration. Structure-Preserving Algorithms for Ordinary Differential Equations*. Springer, 2nd edition, 2006.
- [15] C. Hartmann. An ergodic sampling scheme for constrained Hamiltonian systems with applications to molecular dynamics. *J. Stat. Phys.*, 130(4):687–711, 2008.
- [16] C. Hartmann, C. Schütte, and W. Zhang. Jarzynski equality, fluctuation theorems, and variance reduction: Mathematical analysis and numerical algorithms. *J. Stat. Phys.*, 175(6):1214–1261, 2019.



- [17] R. Hartshorne. *Algebraic Geometry*. Graduate Texts in Mathematics. Springer New York, 2010.
- [18] W. K. Hastings. Monte Carlo sampling methods using Markov chains and their applications. *Biometrika*, 57:97–109, 1970.
- [19] F. Legoll and T. Lelièvre. Effective dynamics using conditional expectations. *Nonlinearity*, 23(9):2131–2163, 2010.
- [20] B. Leimkuhler and R. Skeel. Symplectic numerical integrators in constrained hamiltonian systems. *Journal of Computational Physics*, 112(1):117–125, 1994.
- [21] B. J. Leimkuhler and S. Reich. *Simulating Hamiltonian Dynamics*, volume 14 of *Cambridge Monographs on Applied and Computational Mathematics*. Cambridge University Press, 2005.
- [22] T. Lelièvre, M. Rousset, and G. Stoltz. *Free Energy Computations: A Mathematical Perspective*. Imperial College Press, 2010.
- [23] T. Lelièvre, M. Rousset, and G. Stoltz. Langevin dynamics with constraints and computation of free energy differences. *Math Comput.*, 81(280):2071–2125, 2012.
- [24] T. Lelièvre, M. Rousset, and G. Stoltz. Hybrid Monte Carlo methods for sampling probability measures on submanifolds. *Numerische Mathematik*, 143(2):379–421, 2019.
- [25] J. S. Liu. *Monte Carlo Strategies in Scientific Computing*. Springer, first edition, 2008.
- [26] S. Livingstone, M. Betancourt, S. Byrne, and M. Girolami. On the geometric ergodicity of Hamiltonian Monte Carlo. *Bernoulli*, 25(4A):3109–3138, 11 2019.
- [27] J.-M. Marin, P. Pudlo, C. P. Robert, and R. J. Ryder. Approximate Bayesian computational methods. *Statistics and Computing*, 22(6):1167–1180, 2012.
- [28] N. Metropolis, A. W. Rosenbluth, M. N. Rosenbluth, A. H. Teller, and E. Teller. Equations of state calculations by fast computing machines. *J. Chem. Phys.*, 21(6):1087–1091, 1953.
- [29] R. M. Neal. Probabilistic inference using Markov chain Monte Carlo methods. Technical report, Department of Computer Science, University of Toronto, 1993.
- [30] G. O. Roberts and J. S. Rosenthal. Optimal scaling of discrete approximations to Langevin diffusions. *Journal of the Royal Statistical Society: Series B (Statistical Methodology)*, 60(1):255–268, 1998.
- [31] G. O. Roberts and R. L. Tweedie. Exponential convergence of Langevin distributions and their discrete approximations. *Bernoulli*, 2(4):341–363, 1996.
- [32] P. J. Rossky, J. D. Doll, and H. L. Friedman. Brownian dynamics as smart Monte Carlo simulation. *J. Chem. Phys.*, 69(10):4628–4633, 1978.
- [33] C. Schütte. *Conformational Dynamics: Modelling, Theory, Algorithm, and Application to Biomolecules*. Habilitation dissertation, Free University Berlin, 1999.

- [34] J. Skowron and A. Gould. General complex polynomial root solver and its further optimization for binary microlenses. *arXiv preprint*, 1203.1034, 2012.
- [35] A. J. Sommese, J. Verschelde, and C. W. Wampler. Introduction to numerical algebraic geometry. In M. Bronstein, A. M. Cohen, H. Cohen, D. Eisenbud, B. Sturmfels, A. Dickenstein, and I. Z. Emiris, editors, *Solving Polynomial Equations: Foundations, Algorithms, and Applications*, pages 301–337. Springer Berlin Heidelberg, Berlin, Heidelberg, 2005.
- [36] S. Tavaré, D. J. Balding, R. C. Griffiths, and P. Donnelly. Inferring coalescence times from DNA sequence data. *Genetics*, 145(2):505–518, 1997.
- [37] E. Zappa, M. Holmes-Cerfon, and J. Goodman. Monte Carlo on manifolds: Sampling densities and integrating functions. *Commun. Pure Appl. Math.*, 71(12):2609–2647, 2018.
- [38] W. Zhang. Ergodic SDEs on submanifolds and related numerical sampling schemes. *ESAIM: Math. Model. Num.*, 54(2):391–430, 2020.
- [39] W. Zhang, C. Hartmann, and C. Schütte. Effective dynamics along given reaction coordinates, and reaction rate theory. *Faraday Discuss.*, 195:365–394, 2016.